Mansoura University
Faculty of Engineering
Mansoura Engineering Journal

Investigation of Air Flow Over Delta and Cranked Arrow Delta Wings

دراسة سريان الهواء حول جناح مثلث و جناح مثلث منكسر الأضلاع

A. M. Draz, *H. M. El Saadany*, *M. M. Awad* and W. M. El Awady

KEYWORDS:
Delta Wing, Cranked Arrow Delta Wing, Angle of Attack, Span, Chord, Lift Coefficient, Drag Coefficient, Vortex Breakdown.

الملخص العربي: **يقدم لنا البحث دراسة عددية باستخدام برنامج ميكانيكا الموائع الحسابيه (ANSYS 15) لمقارنة شكلين من أشكال الأجنحة المثلثة وهي شكل الدلتا البسيط و شكل جناح الدلتا المنكسر الأضلاع. تمت الدراسة في مدى زوايا هجوم من 5° إلى 65° عند رقم ماخ يتراوح بين (0.15 إلى 1.4). وأوضحت النتائج أنه في حالة السرعات الأقل من سرعة الصوت (رقم ماخ من 0.15 إلى 0.8) أن معامل الرفع (C_L) يزداد بنحو 25% في حالة الجناح المنكسر مقارنة بالجناح البسيط في حين تتناقص قوى الإعاقه لسطح الجناح المنكسر نتيجة للنقص في مساحته بمقدار 7%. وفي حالة السرعات الأعلى من سرعة الصوت (رقم ماخ 1.2 ,1.4) فإن معامل الرفع (C_L) يزداد بمقدار حوالي 15% في حالة الجناح المنكسر بالمقارنة بالجناح البسيط مقابل زيادة في معامل الإعاقه (C_D) بمقدار لا يتعدى 2%. في كلا الشكلين زيادة رقم ماخ يؤدي إلى زيادة معامل الرفع في حالة السرعات الأقل من سرعة الصوت وتناقص في معامل الرفع عند السرعات الأعلى من سرعة الصوت. ومعدل التغير يزداد في حالة الجناح المنكسر. وكذلك فإن توزيع الضغوط على سطح الجناح المنكسر أكثر انتظاماً. ومن ذلك يتضح أن أداء الجناح المنكسر أفضل من أداء الجناح البسيط مما يعطيه أفضلية في حالة الطيران والمناورة.**

***Abstract*— Delta wing shapes are unique in their structure advantages and aerodynamic characteristics. On supersonic designing, a delta wing shape is often used to reduce drag and achieve the optimal performance. In this study, a commercial software (ANSYS 15) is used to investigate the performance of two delta wing shapes (simple delta wing and cranked arrow delta wing) at different angles of attack (5° to 65°) and different flow speeds (M = 0.15 to 1.4) in order to obtain the lift and drag coefficients, pressure distribution around the investigated wings, and velocity filed. The results indicate that: (*i*) at *subsonic speed* (M = 0.15 to 0.8), the lift coefficient for the cranked arrow delta wing increases by about 25%. While the drag coefficient in case of cranked arrow delta wing increases by a value reaches 5%, as the area of the cranked arrow delta wing is less by about 7%, this leads to decreasing drag force for the cranked arrow wing, which improves its performance. The lift and drag coefficients increase with increasing Mach number, the rate of increase is higher in the cranked arrow delta wing. In cranked arrow delta wing, vortex breakdown is delayed than that in simple delta wing, which makes the cranked arrow more stable. In addition, the cut parts from cranked arrow at trailing edge help to avoid the effect of vortex breakdown on the wing. (*ii*) At *supersonic speed* (M = 1.2 to M = 1.4), the lift coefficient of the cranked arrow delta wing is higher than that for simple delta wing by about 15%, while the increase in the drag coefficient does not exceed 2%, which increases cranked arrow wing's performance. The lift and drag coefficients decrease with increasing Mach number, the rate of decrease is higher in the cranked arrow delta wing. In the cranked arrow delta wing as Mach number increases, a better pressure distribution over the wing surface is observed which improves the stability during flight and maneuvering.**

Received: (19 November, 2019) - Revised: (7 May, 2020) - Accepted: (23 June, 2020)

A. M. Draz is a mechanical power engineer (eahmeddraz@gmail.com).

H. M. El Saadany, Professor at Mechanical Power Engineering Department. Faculty of Engineering, Mansoura University, (Hmsaadny@yahoo.com).

M. M. Awad, Associate Professor at Mechanical Power Engineering Department, Faculty of Engineering, Mansoura University, (m_m_awad@mans.edu.eg.com.).

W. M. El Awady, Assistant Professor at Mechanical Power Engineering Department, Faculty of Engineering, Mansoura University, (welawady@mans.edu.eg)

I. INTRODUCTION

At low speeds, delta wings generate higher lift than rectangular planform wings, which improves its performance. A better drag characteristic at supersonic is a result of using delta wing. In addition, delta wings have a structural advantage over rectangular planform wings and easy to be manufactured. While cranked arrow has a high sweep inboard panel for low drag at supersonic speeds and a low sweep outboard panel to provide better handling and maneuverability at subsonic speeds (Houghton and Carpenter [1]). The simple and cranked arrow wings are used in the applications of supersonic and transonic aviation due to its aerodynamic performance and maneuverability at high angles of attack. These advantages are due to the vortex generated from the strake wing (or the inboard wing) stabilizes the flow on the main wing (or the outboard wing), while the outboard wing leading edge has a smaller sweepback angle than that of the inboard wing which increases the wing aspect ratio as a whole and low-speed performance is improved. Another issue with the cranked delta wings is its tendency to pitch up at high angles of attack to become stiffer and stronger, where the loads are highest (Stanbrook and Squire [2]). Earnshaw [3] studied the formation of the leading-edge separation vortex that occurs on wings with sharp and highly swept leading edges. He divided the vortex structure into three regions: (*i*) the outer (free shear) layer, (*ii*) the rotational core, which represents the outer layer of the vortex core, and (*iii*) the viscous sub-core located within the rotational core. Hummel and Srinivasan [4] and Wentz and Kohlman [5] studied vortex breakdown over a delta wing with flat plate surface and leading edge sweep angles between 45º-85º at low-speed with varying aspect ratio to determine breakdown location with different angles of attack. They found that: with increasing sweep angle, the vortex breakdown occurs at a higher angle of attack. The breakdown first occurs in the wake near the wing trailing edge and moves upstream towards the apex, as the angle of attack is increased and vice versa: as the angle of attack decreases, the breakdown moves back downstream. As the breakdown occurs, both the tangential and axial velocities related to vortex flow decrease, causing a reduction of lifting over the wing as well as a reduction of nose-down pitching moment, which leads to a delta wing stalling. Finally, low angles of attack cause a delay in flow separation, while higher angles of attack cause a delay in vortex breakdown.

Sforza and Smorto [6] experimentally found that, for a delta wing at the low-speed flow and highly swept angle with sharp leading edges and high angle of attack, there is no vortex axisymmetric and no scale linearly within half of the span or in the region of the axis of vortex rotation. In addition, they found that viscous character becomes important as maximum flow velocity decreases with downstream distance. Gad-El-Hak and Blackwelder [7] observed that free stream flow over the primary vortices is redirected towards the wing and suddenly swept outboard below the primary vortices which create a smaller and weaker secondary vortex that rotates in an opposite direction to the primary vortex; hence the secondary vortex forced the primary vortex to move upward and inboard. Konstadinopoulos et al. [8] experimentally studied subsonic wing rock of slender delta wings and they reported that: the self-excited motion of a flat delta wing was free to roll about an axis parallel to its mid-span chord. In addition, they stated that the symmetric configuration of the leading-edge vortex system becomes unstable as the angle of attack increases. Gad-el-Hak and Ho [9] studied pitching of delta wing and found that: steady flow can provide high lifting at large angles of attack; therefore, it can be used in many high-performance aircraft and the unsteady aerodynamic properties of a delta wing are practical. Mehta and Cantwell [10] experimentally studied the main and turbulent properties of a single longitudinal vortex generated by a half-delta wing at subsonic speed. They illustrated that: the initially distorted vortex at a stream wise station equivalent to a half wing height become rounded by about triple wing height, while in this transition region the interaction between primary, secondary and even tertiary vortices help the peak vorticity dropped by about 50%. The Particle Image Velocimetry (PIV) is a new technique used by Cenedese et al. [11]. They measured the velocity field in the wake of a delta wing using optical measurement techniques, which were compared with the Laser Doppler Anemometer. In addition, they measured and focused on the velocity and the primary vortex over the upper and the lower delta wing flows as well as secondary vortices originated from the three-dimensional separation of the flow stream. Yang et al. [12] numerically investigated the flow on the upper surface of the delta wing changes significantly in a wide range of the angle of attack and they concluded that for the vertical flow at a moderate angle of attack, the secondary and tertiary vortices are weakened and the total lift remains unchanged. Rinoie [13] indicated the benefits of the rounded leading-edge vortex flaps on improving the lift/drag ratio of delta wings. Jones and Nakamura [14] investigated the dynamics of the vortex core during pitching of a high-sweep delta wing with pitch-up of a 70° sweep delta wing computationally. They observed that: the dynamics of the vortex core started near the wing leading edge during transitions to vortex breakdown. Furman and Breitsamter [15] experimentally studied the flow over a 65° swept delta wing as part of the (International Vortex Flow Experiment). They used low-speed wind tunnel facilities and laser light sheet flow visualization. They obtained main and unsteady, surface pressure distributions, as well as main and turbulent velocity components of the flow field close to the wing surface. Rahman et al. [16] studied the aerodynamic behavior of the delta wing with 70° degree sweep both experimentally and numerically using the commercial computational fluid dynamics (CFD) code (ANSYS FLUENT-14) at different angles of attack. They predicted the main primary vortex core that provides the main suction peak on the upper surface of the wing. Ruffles and Dakka [17] numerically studied the aerodynamic flow characteristics over a wide range of Mach number in subsonic and supersonic using the CFD. The study included two types of wings, a simple delta wing, and a leading edge root extension (LERX) delta wing. They

concluded that: LERX induces large vortices which create pressure drag and increase lifting more than that in case of the simple delta wing. Sutrisno et al. [18] studied the flow characteristics around canard-delta wing, including the fuselage effect on lift, drag, pitching momentum, vortex center and the strength of negative surface pressure and its trajectory. Where the results of comparison. Baldacchino et al. [19] compared both experimental and theoretical results for the same tested aerofoils, (Delft-designed 30% thick DU97W300 airfoil and an 18% NTUA T18 airfoil) in the same conditions and they indicated that: experimental data were more accurate over a wide range of subsonic and supersonic than theoretical data using CFD. The tip vortex and laminar separation bubble interaction with different aspect ratios and low Reynolds numbers using an experimental method were studied by Genc et al. [20]. They indicated that: with an increasing angle of attack, wing tip vortices become larger and displaced towards the wing leading edge.

Aerodynamic characteristics at subsonic and supersonic speed for different types of delta wing are the subject of the present study. The present study is concerned with two types of the delta wing (simple delta wing and cranked arrow delta wing), which have the same chord, span and thickness ratio at the same flow conditions.

A theoretical study using CFD is to be performed to obtain the pressure distribution, flow velocity, lift and drag coefficients and lift to drag ratio for each wing at different Mach numbers and different angles of attack.

II. MODELING

A. Modeling geometry

The geometry models are shown in Fig. (1), which are the delta wings (simple delta wing and cranked arrow delta wing). The two shapes have the same root chord of *120 mm* and the same span of *112 mm.* The two wings have a *0.083* wing thickness ratio based on each chord length, the same bevel angle of *30°* and the leading edge sweep angle variance around *65°*. The leading edge is sharp in both wings. The trailing edges are straight in simple delta wing and a broken line in cranked arrow delta wing. The upper and lower surfaces are flat to reduce the effect of the leading edge shape on flow fields. The flow field is assumed to be symmetric about the centerline of the wings. The simple delta wing has a surface area of *6720 mm*^{2}, with an aspect ratio of *1.87*, Fig. (1-a). The cranked arrow delta wing has a surface area of *6223 mm*^{2}, with an aspect ratio of *2.02*, the apex of the cranked wing partitions started at *85 mm* from the apex of the delta wing as shown in Fig. (1-b). The wings are to be located in a wind tunnel, as shown in Fig. (2). As Altman [21] implied, with a delta wing, it is more likely to run into solid and wake blockage issues than wall corrections. This is because the governing model span to tunnel span generally is not to exceed 80%. If the ratio equals to or more than this value, wall corrections must be performed. In the present study, the wind tunnel dimensions are taken as (300mm*326mm*988mm) which give a span to wind tunnel span ratio equals to 40%.

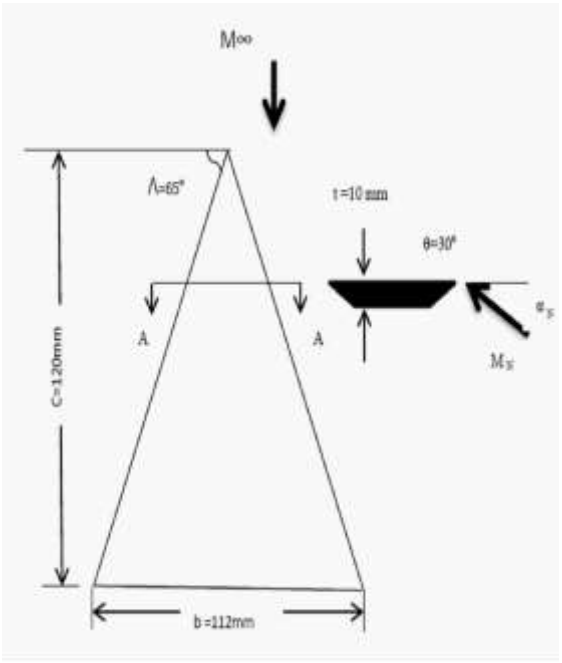

(a) Simple delta wing

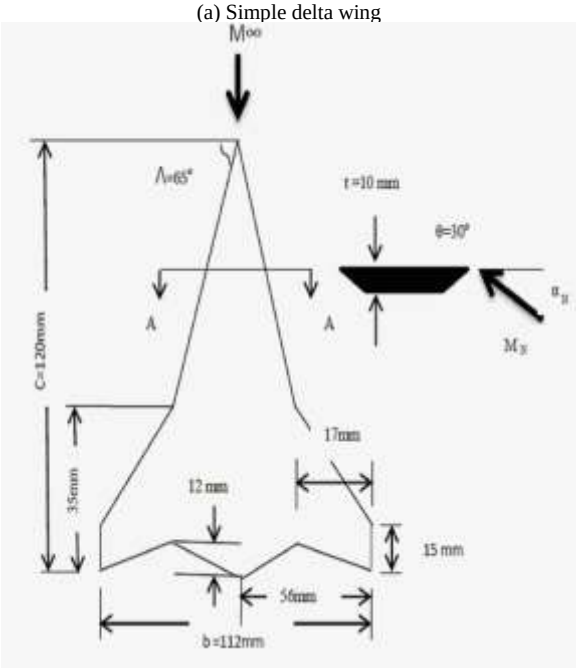

(b) Cranked arrow delta wing

Figure (1) Two types of the delta wing

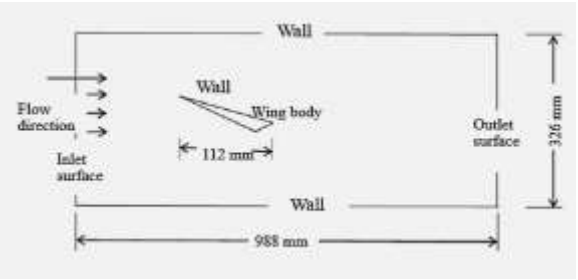

Figure (2) Delta wing located in wind tunnel

According to Altman [21], the study avoids solid blockage and wall corrections in flow through the wind tunnel.

B. Mathematical modeling

The state of motion of a delta wing is determined by its weight, and the thrust force which acts on the wing during its motion. This study will take into consideration the following assumptions; (*i*) one phase laminar flow with a direction parallel to the aerofoil chord line, (*ii*) the free stream flow conditions are constant, (constant temperature, constant pressure, and constant velocity), and the wing material remains in elastic zone, (*iii*) fluid shear is expressed in terms of a constant friction coefficient (unsteady shear stress is neglected), and (*iv*) finally, no rolling or yaw occurs.

The study analyzes forces, velocity distribution and pressure distribution acting on two types of wings using CFD (ANSYS 15). The simulation is done using FLUENT over ANSYS workbench, the solver uses pressure based type, absolute velocity formulation and steady time. The model depends on viscous-Spalart-Allmaras (Rathore [22]) one equation which valid for subsonic and supersonic flow. Also, it takes into consideration the wing material and fluid flow properties as aluminum and air, respectively. The boundary condition at the inlet surface as mass flow calculated based on inlet flow velocity. The calculation of the interior solid media and the outlet condition depends on outlet pressure with a default value equals to the absolute atmospheric pressure. The computation started from the inlet surface which has a simple scheme pressure-velocity coupling with the following special discretization: least squares cell based, gradient and secondary order pressure, density momentum and modified turbulent viscosity. Finally, the program monitors for the lift and drag coefficients (C_L, C_D), lift and drag forces, pressure and velocity distribution.

Lift force is obtained by integrating ΔP perpendicularly to free stream over the wing surface area, to get the following relation for lift force (Houghton and Carpenter [1]):

L = Lift = component of force perpendicular to U_∞
where U_∞ is the free stream velocity

$$C_L = \frac{L}{\frac{1}{2}\rho U_\infty^2 c^2 \tan\Lambda} = 2\pi \tan\Lambda \sin\alpha \cos\alpha$$

$$C_L = \frac{L}{q_\infty S} \qquad (1)$$

where q_∞ is the local flow at free stream speed, S is the wing surface area, Λ is a swept angle, c is the main chord and α is the angle of attack.

Pohlhamus [23] explained how vortices contribute to lift the slender delta wing as seen in Fig. (3). He investigated that at higher angles of incidence, the potential-flow, replaced by a separated flow construction is similar to that for the real flow around a flat plate perpendicular to the oncoming flow. In addition, the summation of both represents the total lift force:

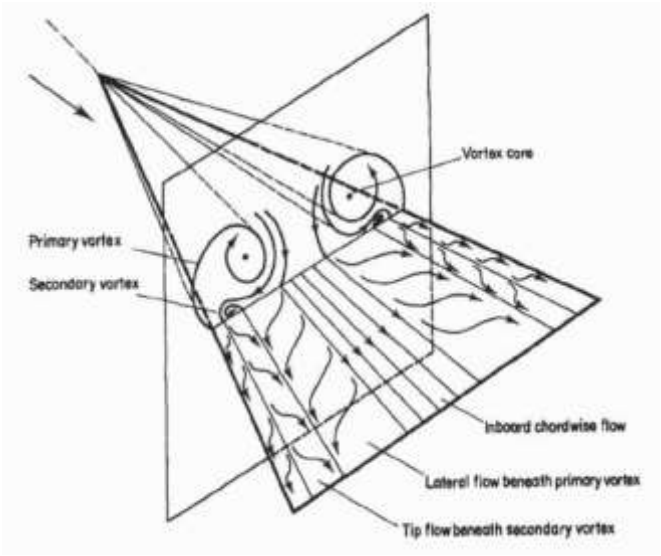

Figure (3) Real flow field around a slender delta wing, showing vortex structure and surface flow pattern (Pohlhamus [23]).

$$C_L = \frac{K_P \sin\alpha \cos\alpha}{Potential\ Flow\ Lift} + \frac{K_V \sin^2\alpha \cos\alpha}{Vortex\ Lift} \qquad (2)$$

where K_p and K_V are coefficients which approximately equal ($2\pi \tan\Lambda$).

Also, the drag force is obtained by integrating the pressure difference in the same direction of the free stream over the wing surface area (Houghton and Carpenter [1]).

D = Drag = component of force parallel to U_∞

$$C_D = \alpha C_L = \frac{2C_L^2}{\pi (AR)^2}$$

$$C_D = \frac{D}{q_\infty S} \qquad (3)$$

The aerodynamic forces and moments affected on the wing body are due to two basic sources; the pressure distribution over the body surface and shear stress distribution over the body surface. Both pressure P and shear stress τ have dimensions of force per unit area. P acts normal to the surface and τ acts tangentially to the surface. Then, the dimensionless Pressure coefficient is (Houghton and Carpenter [1]):

$$C_P = \frac{(P - P_\infty)}{q} \qquad (4)$$

C. Boundary conditions

The air is used as a fluid which flows around the model with a constant temperature of 25°*C*, constant density ρ=1.225 *kg/m*^{3}, and constant dynamic viscosity μ=1.789*10^{-5} *Pa.s*. Also, in the far field taken, the air density ρ_∞= 1.225 *kg/m*^{3}, μ_∞=1.789*10^{-5} *Pa.s*, and P_∞=101325 *Pa*, with different free stream velocities [51 (0.15M), 138 (0.6M), 276 (0.8M), 415 (1.2M), 484 (1.4M)

m/s] according to test conditions. The air exhausted to atmospheric pressure without any backpressure effect. The velocity components in the (*x*, *y*, *z*) directions are separated into the free stream and perturbation components, i.e.

$$\left(U_\infty \cos\alpha + u', U_\infty \sin\alpha + v', w'\right) \quad (5)$$

III. MESH STUDY

In the present study, ANSYS-15 (CFD) is to be used to perform the required numerical study. The pressure distribution, velocity distribution, drag and lift forces, and pressure and drag and lift coefficients are to be calculated. A mesh study was done in order to obtain the proper number of nodes and cells and growth rate in the case of structured and unstructured grids. The numerical results of Oyama et al. [24] and experimental results of Miller and Wood [25] are chosen to be the base of comparison between structured and unstructured grids. In the case of structured mesh, the results of the pressure coefficient versus dimensionless chord distance was found to achieve stability when the number of nodes equals 1,750,000 using 1,195,000 elements with running time equals 50 minutes. On the other hand, using the unstructured meshing, stability was achieved at a number of nodes equal 88,000 using 92,000 elements at a growth rate (1.1) with running time equals 25 minutes. The results of this study are shown in Fig. (4) at different values of Mach number and angle of attack.

By calculating the degree of congruence, an error analysis was performed according to the following equation, Sawheny [26]:

$$\text{Error} = \sqrt{\frac{\sum_{i=1}^{n} (Experimental\,Value - Theoretical\,Value)^2}{N-1}} \quad (6)$$

In the case of structured meshing an error reaches 10% with respect to the experimental results of Miller and Wood [25], while it reaches 4.6% in the case of unstructured meshing. Therefore, in the present study, the unstructured meshing will be used with the number of nodes 88,000 and number of elements 92,000 and growth rate equals 1.1 since it has higher accuracy and lower running time.

IV. RESULTS AND DISCUSSION

In the present study, the CFD results for pressure distribution, flow velocity, lift, and drag coefficients were obtained for both simple delta wing and cranked arrow delta wing at different Mach numbers,(M_∞ = 0.15, 0.4, 0.8, 1.2, 1.4) and different angles of attack (5º, 25º, 45º, 65º). Stanbrook and

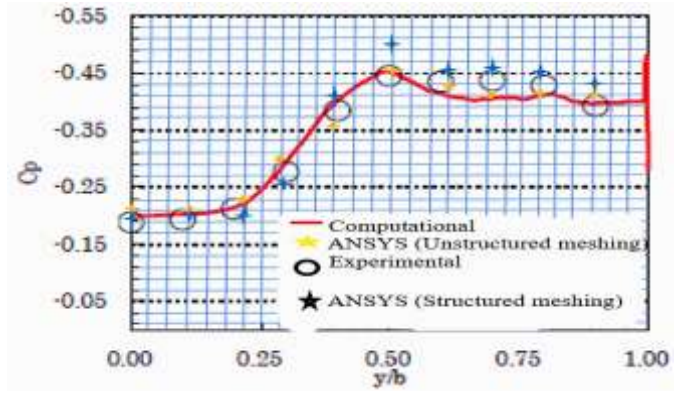

(a) M_∞ =1.7, α =20º

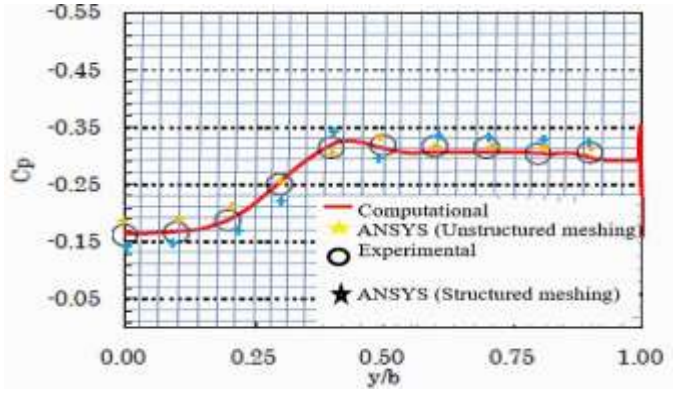

(b) M_∞ = 2, α =20º

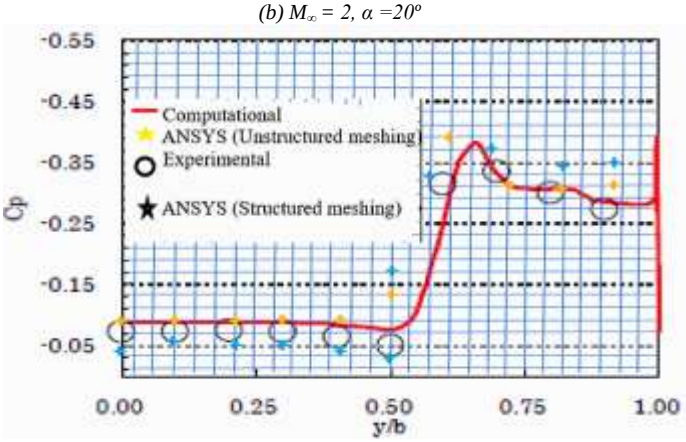

(c) M_∞ = 1.7 α = 8º

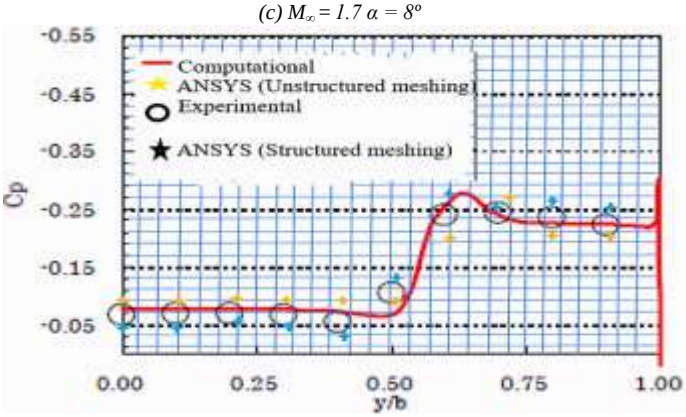

(d) M_∞ = 2, α = 8º

Figure (4) Comparison between present results (structured and unstructured), with Miller and Wood [25], and Oyama et al. [24] at different Mach numbers (M) and different angles of attack (α).

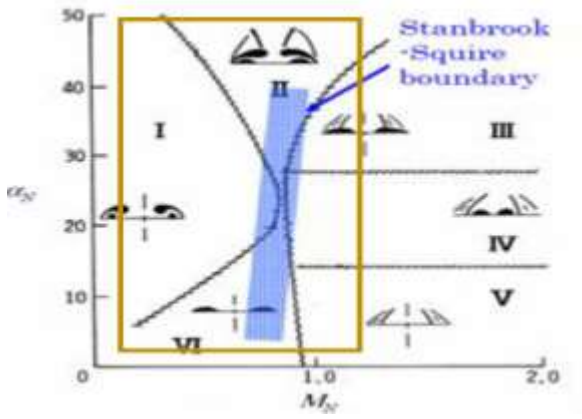

Figure (5) Flow field classification chart by Miller and Wood (Miller and Wood [25])

Squire [2] classified the flow patterns based on the angle of attack normal to the leading edge α_N, and Mach number normal to the leading edge M_N,

$$M_N = M_\alpha \cos(1+\sin^2\alpha \tan^2\alpha)^{1/2} \quad (7)$$

$$\alpha_N = \tan^{-1}(\tan\alpha/\cos\Lambda) \quad (8)$$

into two types; 1) attached flow, and 2) separated flow at the leading edge. The boundary line between two types which exist near (M_N = unity), known as the Stanbrook-Squire [2] boundary, Fig. (5). Miller and Wood [25] experimentally studied the flow characteristics over the delta wing with different leading edge sweep angles, using tufts, oil flow, and vapor screen methods.

The flow was classified into six patterns according to (α_N & M_N), as follows; (I) classical vortex, (II) vortex with shock, (III) shock with separation bubble, (IV) shock-induced separation, (V) shock with no separation, and (VI) no shock with separation bubble. According to the present study, all the obtained results are located in the rectangular zone, shown in Fig. (5). The present results for lift and drag coefficients for both simple delta wing and cranked arrow delta wing are illustrated in Figs. (6) to (8).

As seen from these figures, the cranked arrow delta wing has a less improvement at supersonic speeds in comparison with that at subsonic speeds. In general, the cranked arrow delta wing provides a significant increase in the maximum lift coefficient, and a slight reduction in the drag coefficient at small angles of attack.

The results are illustrated in more details for both subsonic and supersonic cases as follows:

A. Subsonic Speed (M_∞= 0.15 and M_∞= 0.8)

As a sample of the subsonic results, Figs. (6) to (8) show the lift coefficient, drag coefficient and lift to drag coefficients versus several angles of attack and different Mach numbers. For subsonic cases where Mach number ranging from 0.15 to 0.8, it can be observed that, the lift coefficient for the cranked arrow delta wing is higher than that for simple delta wing. This increases the lift forces for the cranked arrow delta wing by a value of bout 25% according to the angle of attack. Also, it can be seen that the drag coefficient in case of cranked arrow delta wing increases by a value reaches 5% than that for simple delta wing. As the area of the cranked arrow delta wing is less by about 7% than that of simple delta wing, this leads to lower drag force for the cranked arrow wing which improves its performance. Stall occurs at an angle of about 40º in case of the cranked wing while in simple delta wing it is about 45º. After stall occurs, lift and drag coefficient for the cranked arrow delta wing is less than lift and drag coefficient for the simple delta wing which makes cranked arrow more safe than the simple delta wing. Stalling is not affected by changing the flow speed, but only affected by the value of angle of attack. A comparison between the present work results and Ruffles and Dakka [17] results is performed for simple delta wing at M=0.25 as shown in Figs. (9). For the drag coefficient, there is a good agreement in both values and trends. While the lift coefficient agrees in trend but it slightly differs from the values of Ruffles and Dakka [17]. The present work stalling angle is 45º, while their stalling occurs at 35º. The difference in result values and stalling is due to the effect of bevel angle which increases vortex height and strength above the upper surface of the wing.

Figures (10) and (11) show the pressure contour on the upper surface of both wings at M=0.15 and M=0.8 at angles of attack 15º, 25º, 35º and 45º. From these figures, it can be seen that as the angle of attack increases for both wings, vortex breakdown moves towards the apex of the wings. Also, as the angle of attack increases, in both types of wings, the main primary vortex radius increases, causing an increase in the pressure difference between the upper and lower surfaces of the wing that actually affect on lift and drag forces.

In the cranked arrow delta wing, vortex breakdown is delayed than the vortex breakdown that occurs in simple delta wing, which makes the cranked arrow more stable than the simple delta wing. Also, the cutting parts from cranked arrow at trailing edge help to avoid the effect of vortex breakdown on the wing.

From Figs. (13) to (20), the pressure variation in the domain around apex of simple delta wing is less than the pressure variation around the apex of cranked arrow delta wing. On the other hand, the pressure variation around the trailing edge of simple delta wing is more than the pressure variation around the trailing edge of the cranked arrow delta wing according to the cutting parts from the cranked arrow, this means that: the cranked arrow is more stable during flight and gives the cranked arrow delta wing more maneuverability than simple delta wing, especially in takeoff and redirection during flight. The broken trailing edge of the cranked arrow delta wing helps to avoid vortex breakdown to occur above the wing area which reduces pressure oscillation.

B. Supersonic Speed (M_∞= 1.2 to M_∞= 1.4)

Referring to Figs. (6) to (8), at the same flow conditions, the lift coefficient for cranked arrow delta wing is higher than that for simple delta wing. This increases the lifting force for cranked arrow by about 15% according to the angle of attack, while the increase in the drag force does not increase than 2% with respect to the simple delta wing, which gives cranked arrow wings higher performance than simple delta wing in the

range of supersonic speed. As the Mach number increases, the lift coefficient decreases and drag coefficient increases, this

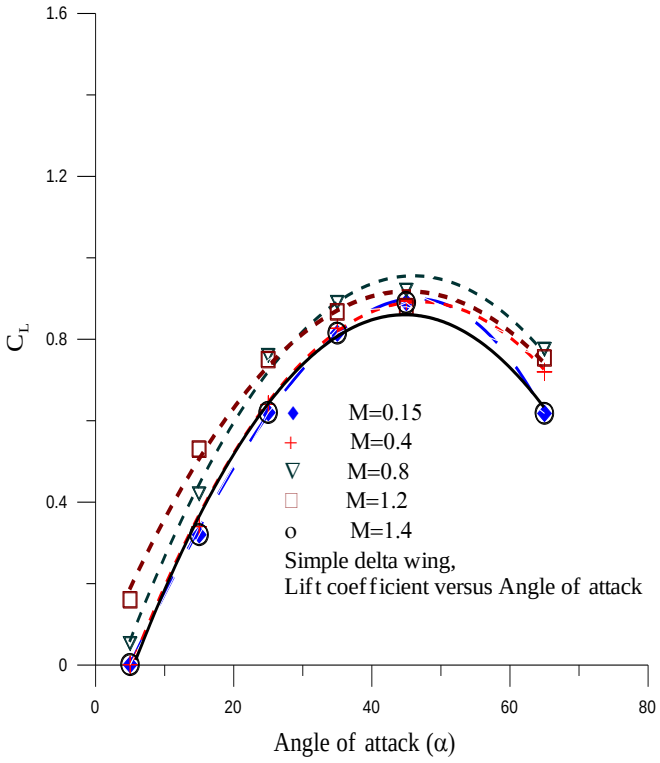

(a) Simple delta wing

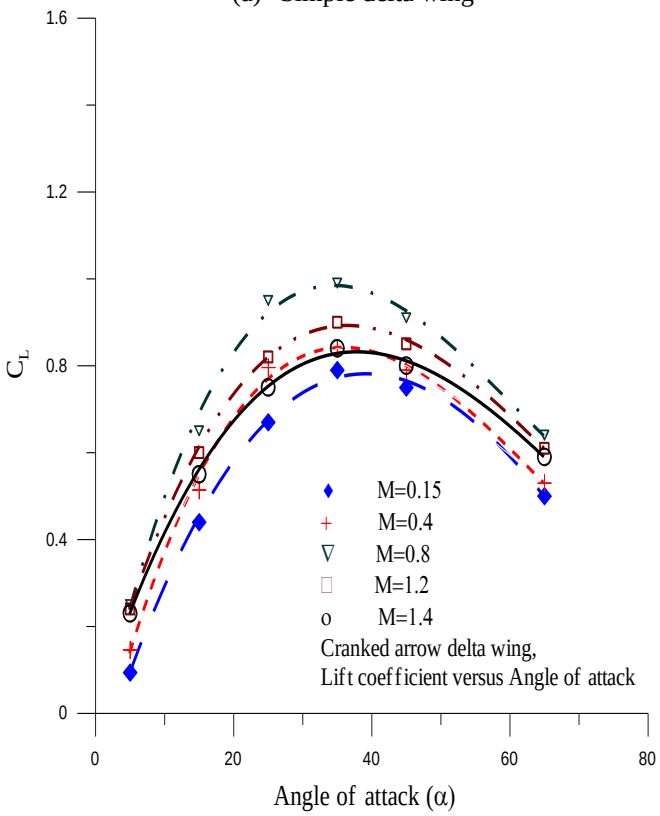

(a) Cranked arrow delta wing

Figure (6) Lift coefficient versus angle of attack at different Mach numbers

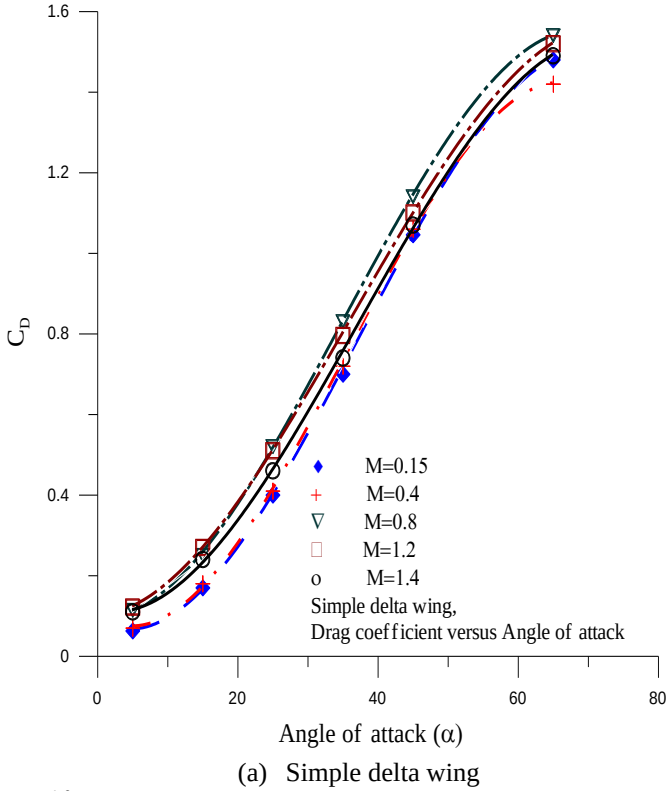

(a) Simple delta wing

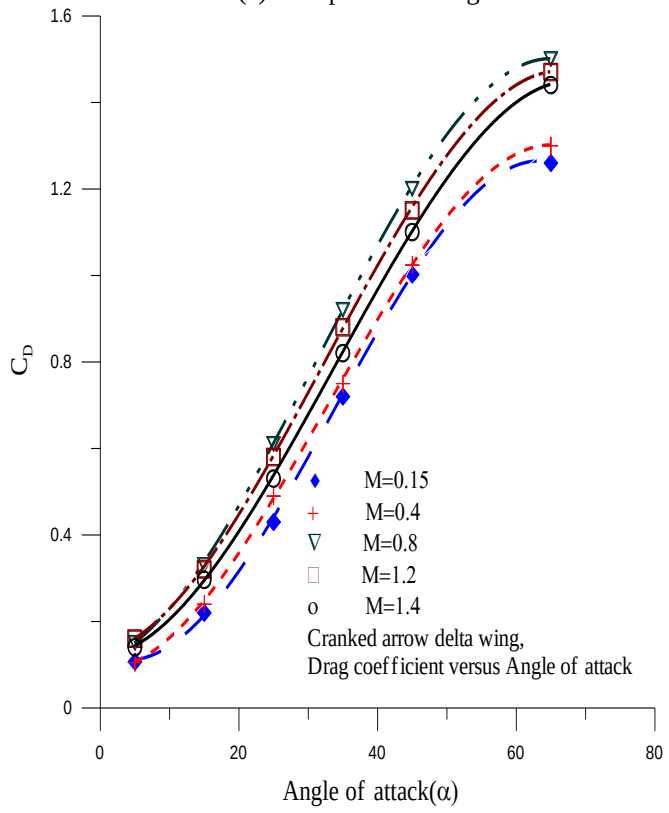

(b) Simple delta wing

Figure (7) Drag coefficient versus angle of attack at different Mach numbers

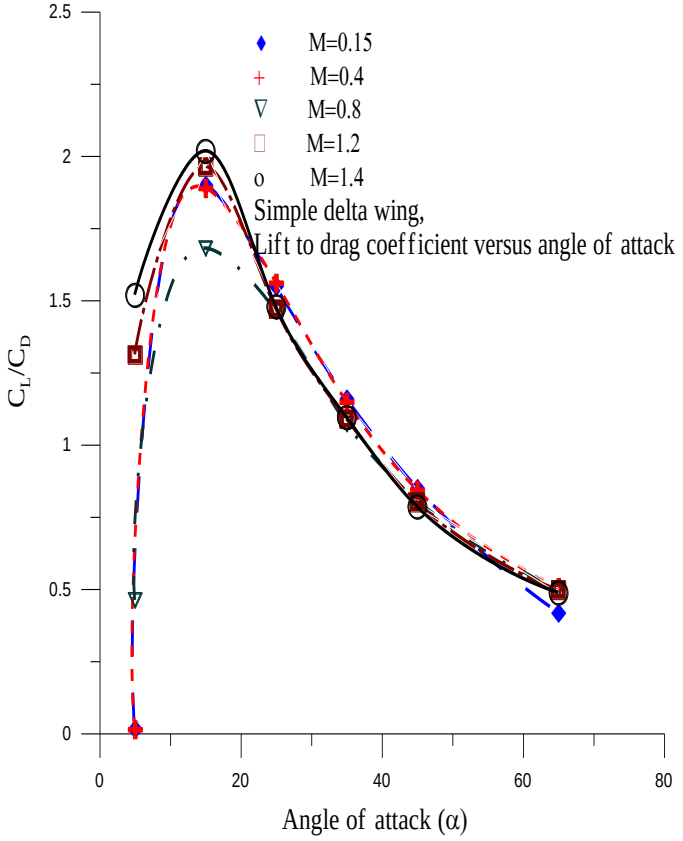

(a) Simple delta wing

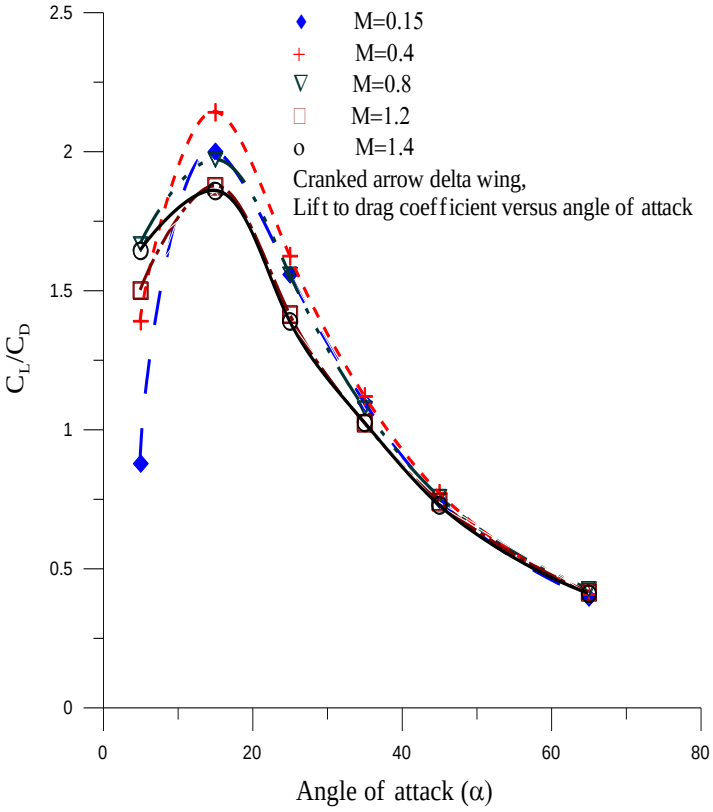

(b) Cranked arrow delta wing

Figure (8) Lift to drag coefficient ratio versus angle of attack at different Mach numbers

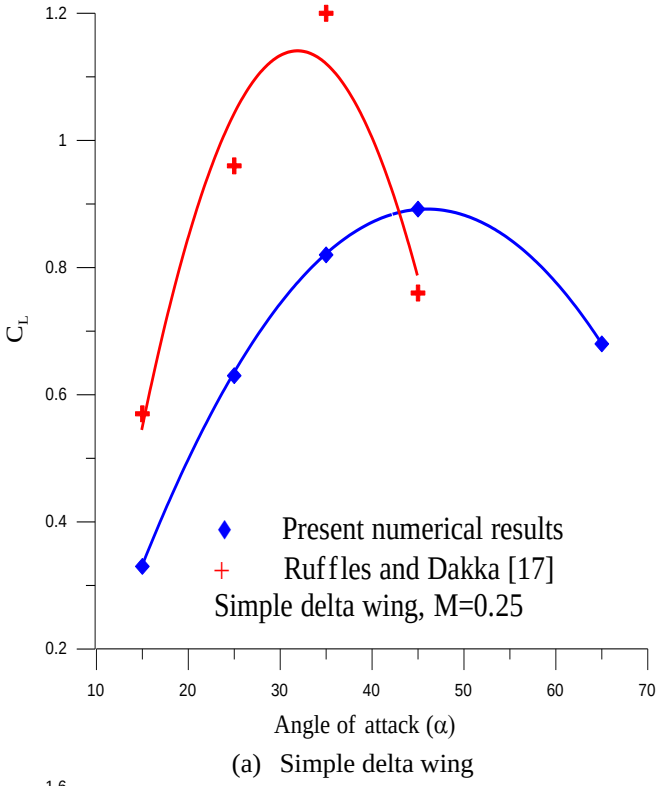

(a) Simple delta wing

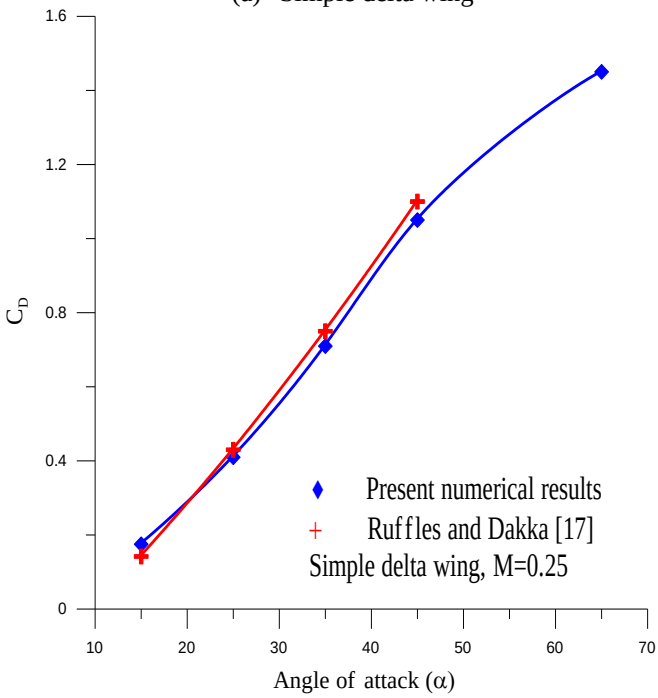

(b) Cranked arrow delta wing

Figure (9) Comparison between present numerical study results and Ruffles and Dakka [17]. (a) C_L versus angle of attack, (b) C_D versus angle of attack

appears clearly in the case of the cranked arrow delta wing, while it is still more than the lift coefficient for the simple delta wing.

Figure (12) illustrates an example of the pressure contour on the upper surface of both delta and cranked wings at different angles of attack at a Mach number (M=1.4). It is

clear that as the angle of attack increases, the vortex core deviates away from the wing surface and the secondary vortex generates and the shear eliminates the primary vortex effect. Also, the pressure distribution on the surface becomes semi-uniform on the upper wing surface.

Figures (21) to (24) show the pressure distribution at MAC line at Mach number, (M_∞ = 1.4) and angle of attack ranging from 15º to 45º for both simple and cranked wings. From these figures it can be shown that: as the angle of attack increases, the pressure difference between upper and lower surface increases and the cranked shape helps to reinforce the vortex above the wing to cover a wide area above the wing and improves the stability during flight and maneuvering which increases the performance of the cranked arrow delta wing. The same results are obtained for the case of Mach number M=1.2, but for the purpose of limiting the figures, the results of M=1.4 were considered only.

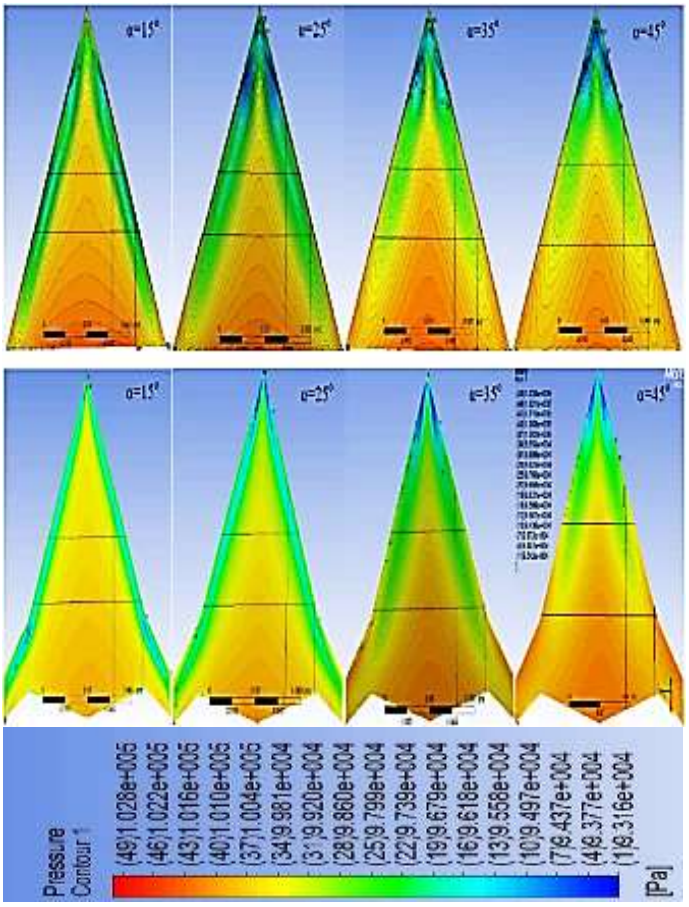

Figure (10) Pressure contour on the upper surface of the simple delta wing and cranked arrow delta wing at M_∞ = 0.15, α = 15°, 25°, 35°, 45°.

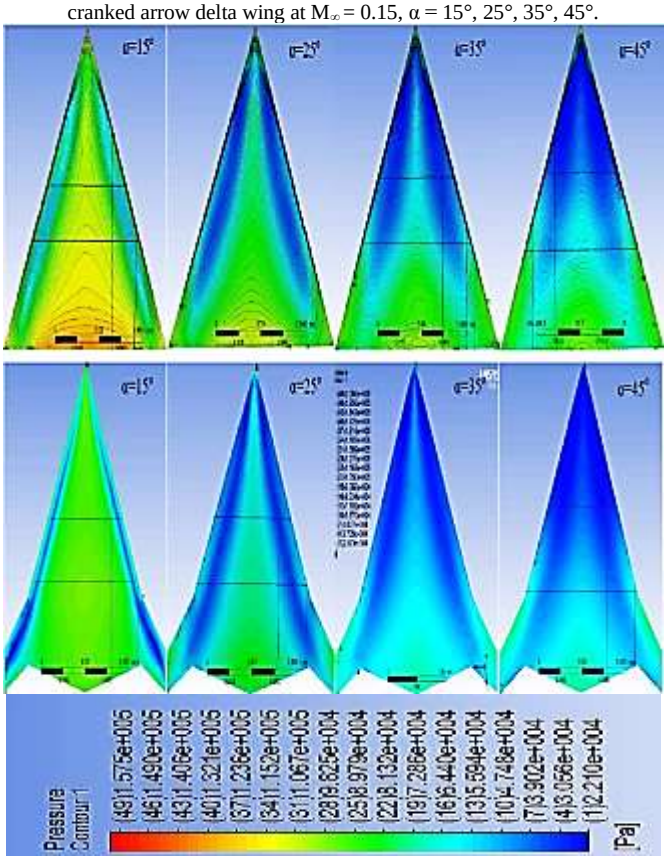

Figure (11) Pressure contour on the upper surface of the simple delta wing and cranked arrow delta wing at M_∞ = 0.8, α = 15°, 25°, 35°, 45°.

The velocity contours at the MAC line for simple and cranked wings at different Mach Numbers and different angles of attack are shown in Figs. (25) to (27). From these figures, the maximum lifting coefficient for cranked arrow increases in case of supersonic than in case of subsonic, while it does not change with an observed value in the case of the simple delta wing.

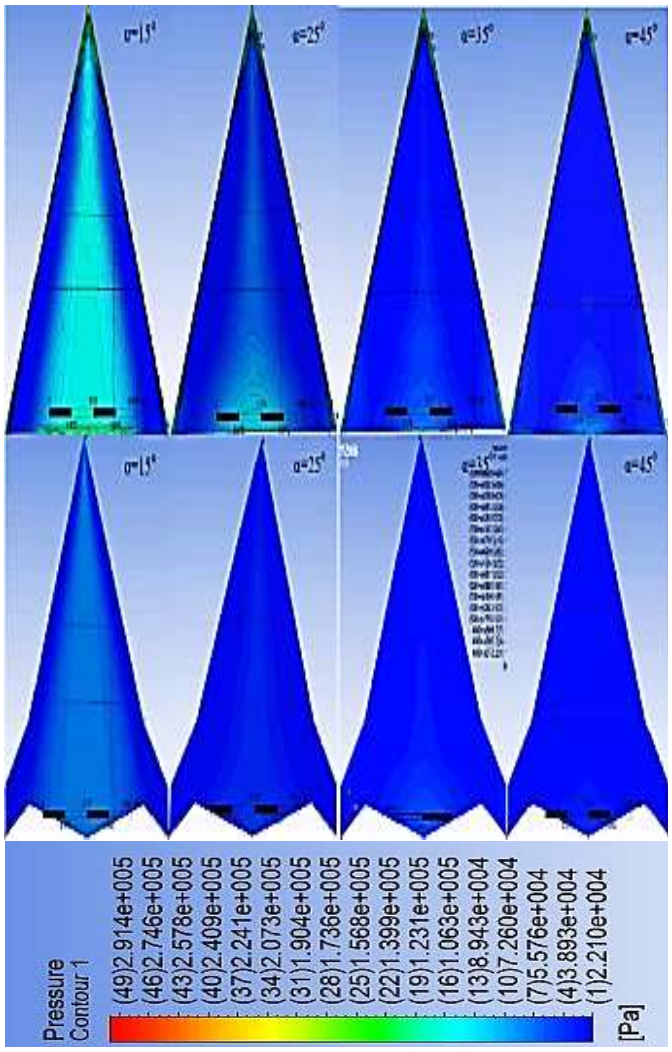

Figure (12) Pressure contour on the upper surface of the simple delta wing and cranked arrow delta wing at M_∞ =1.4, α = 15°, 25°, 35°, 45°

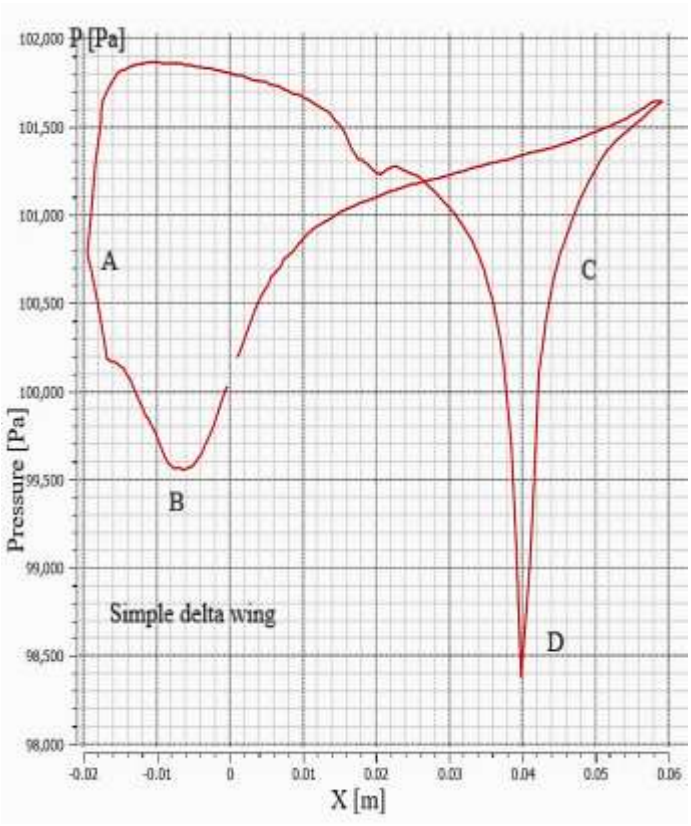

(a)

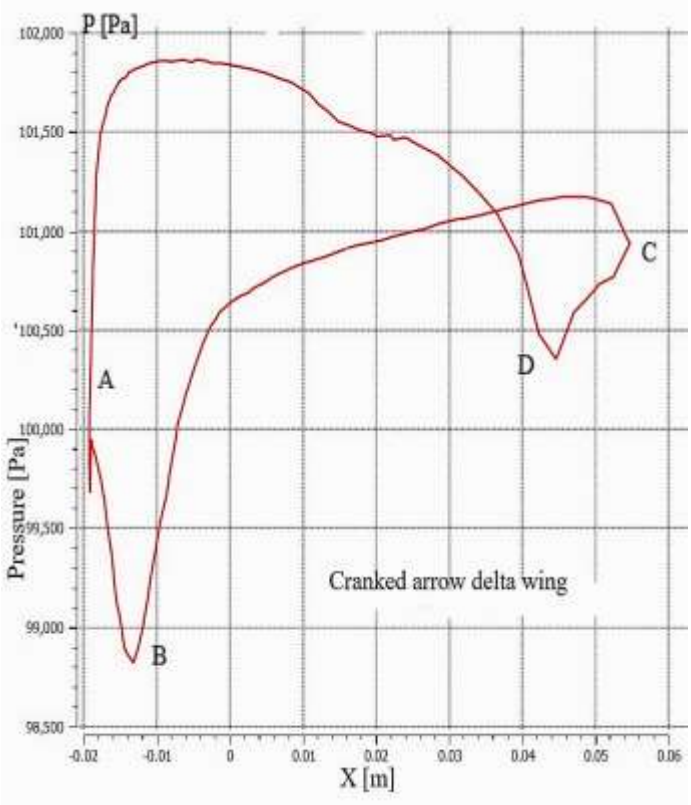

(b)

Figure (13) Pressure distribution at MAC line, α =15°, M_∞ = 0.15

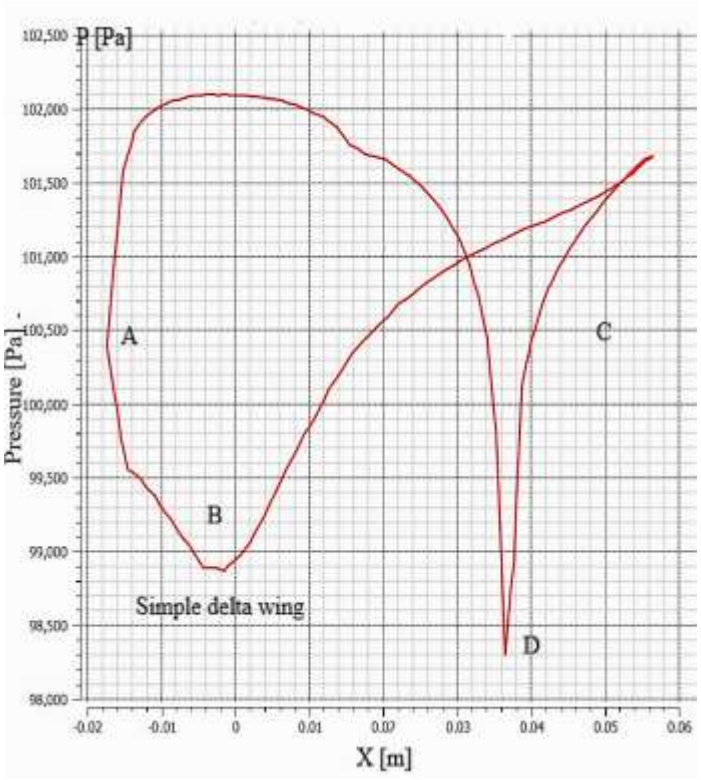

(a)

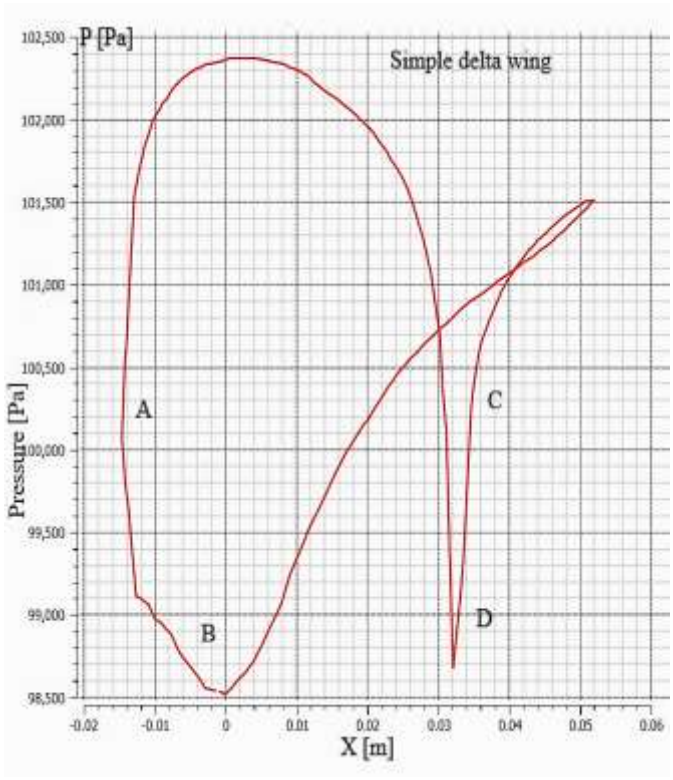

(a)

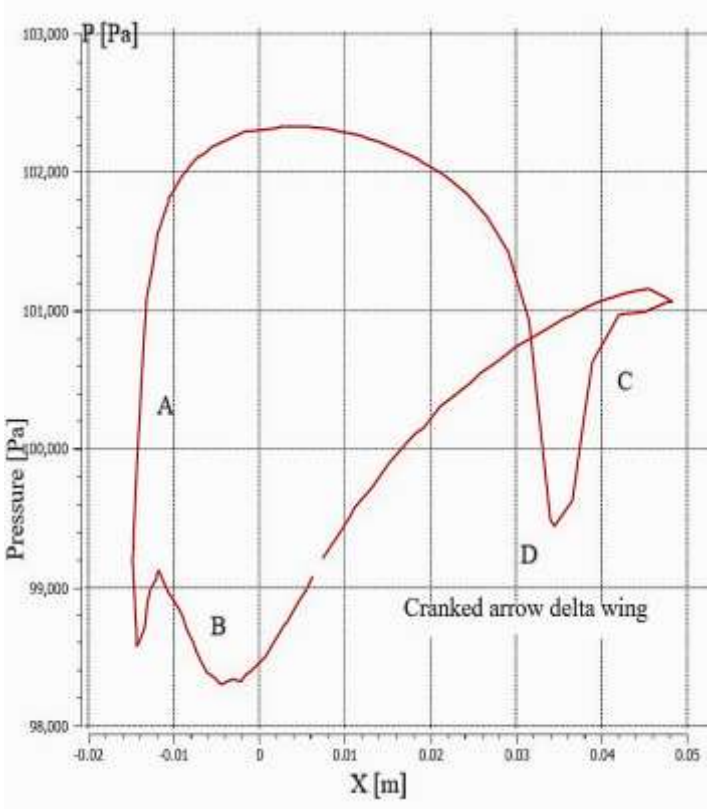

(b)

Figure (14) Pressure distribution at MAC line, α = 25°, M_∞ = 0.15

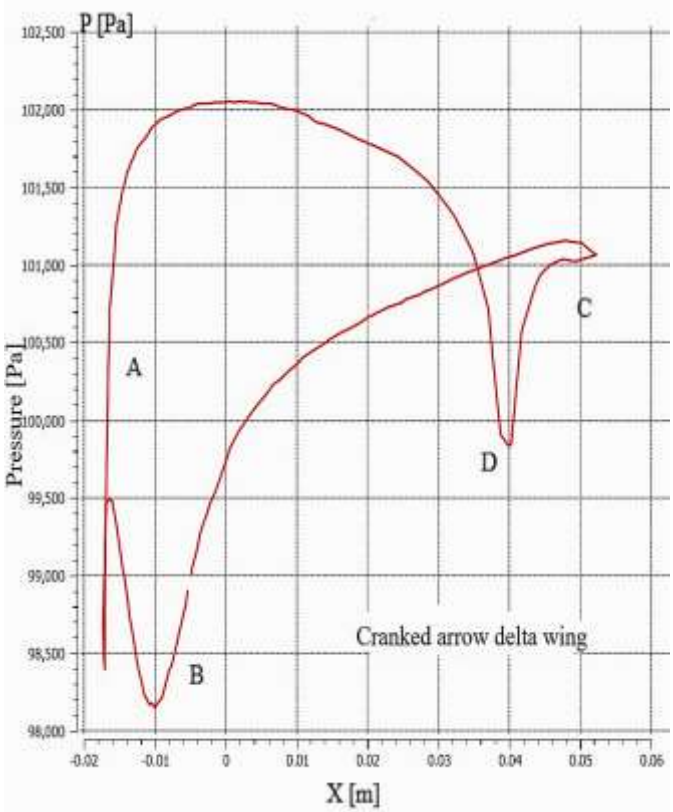

(b)

Figure (15) Pressure distribution at MAC line, α = 35°, M_∞ = 0.15

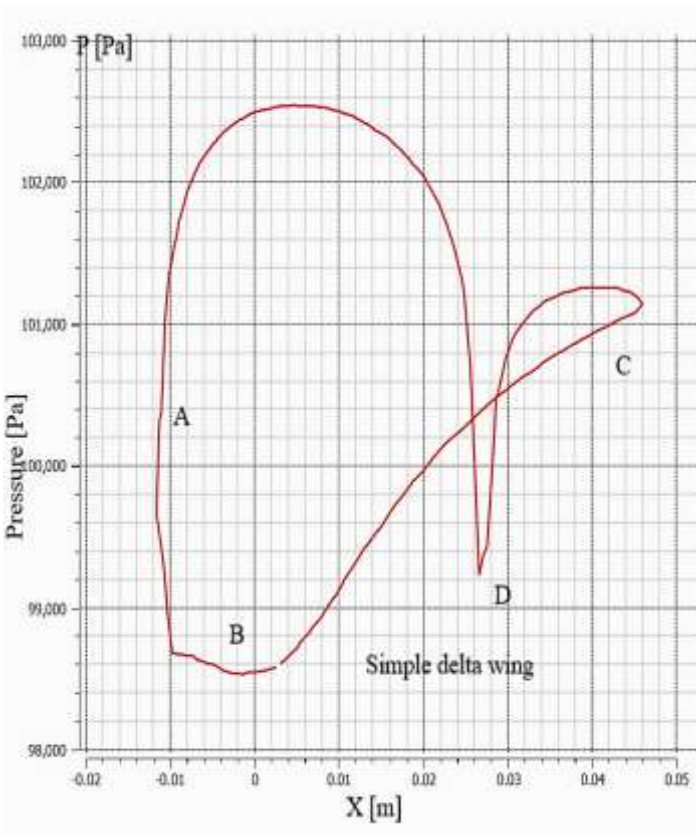

(a)

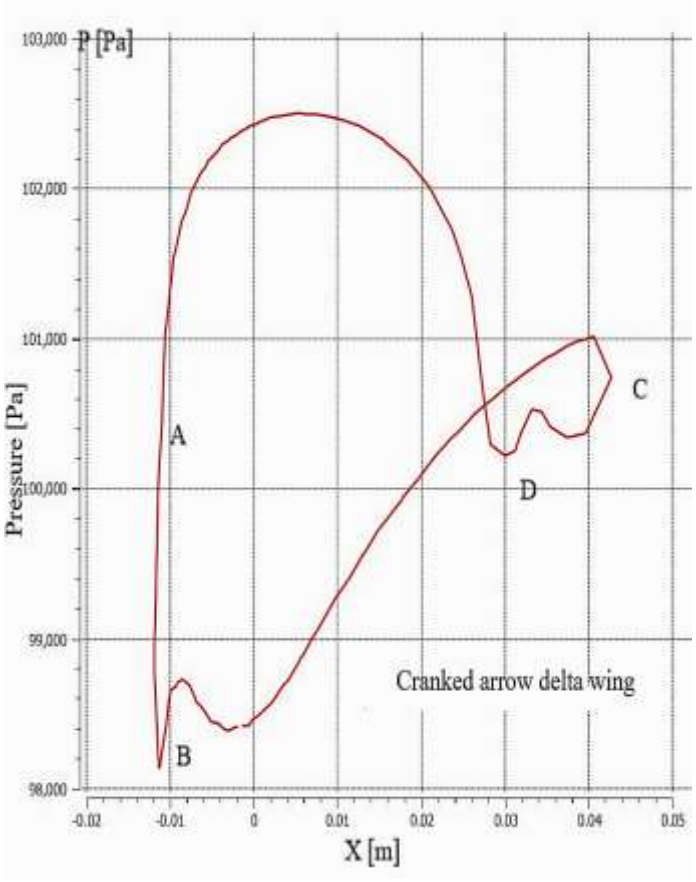

(b)

Figure (16) Pressure distribution at MAC line, $\alpha = 45°$, $M_\infty = 0.15$

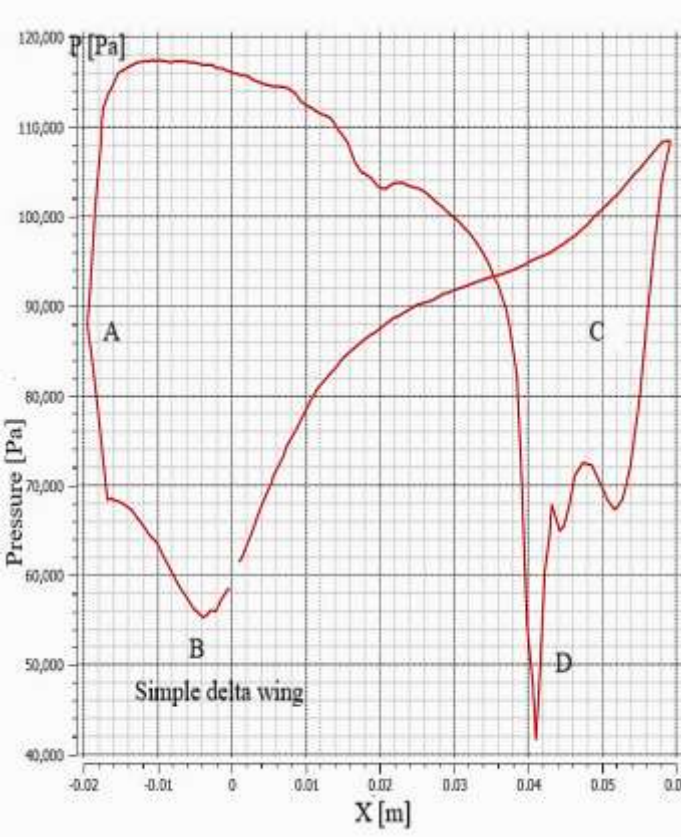

(a)

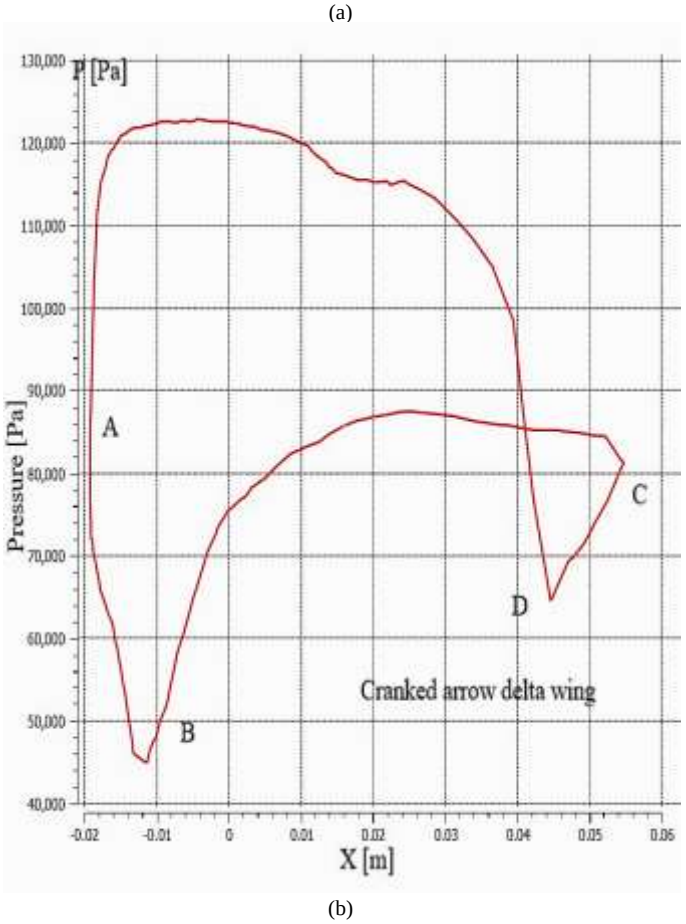

(b)

Figure (17) Pressure distribution at MAC line, $\alpha = 15°$, $M_\infty = 0.8$

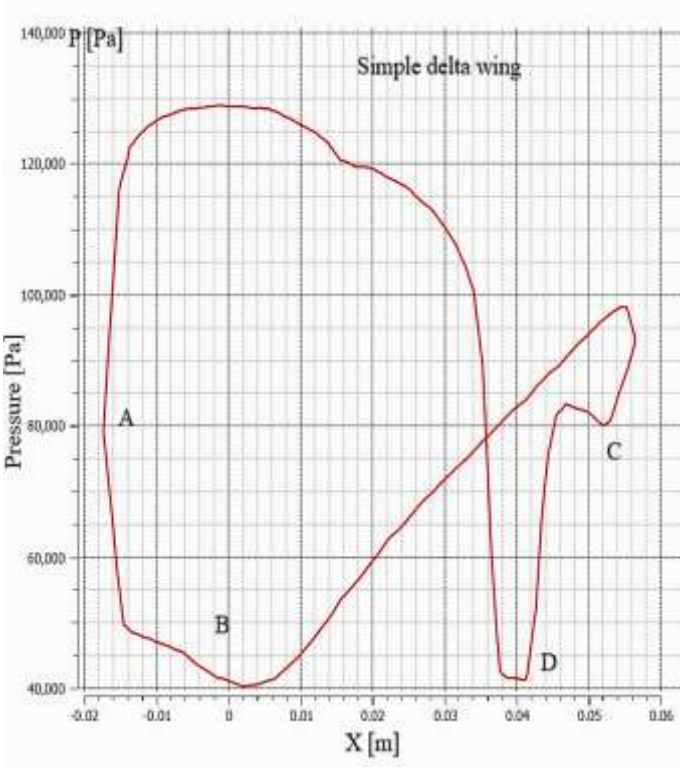

(a)

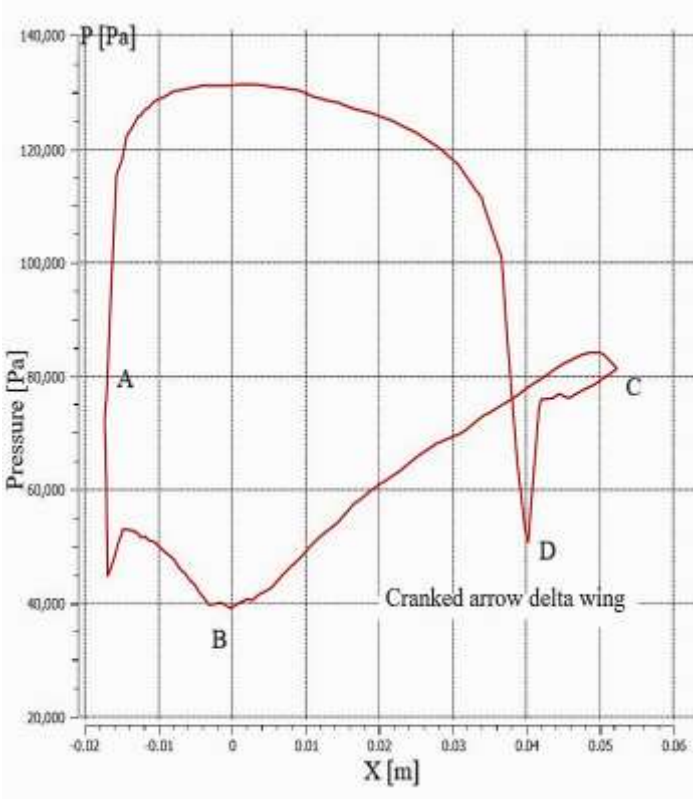

(b)

Figure (18) Pressure distribution at MAC line, $\alpha = 25°$, $M_\infty = 0.8$

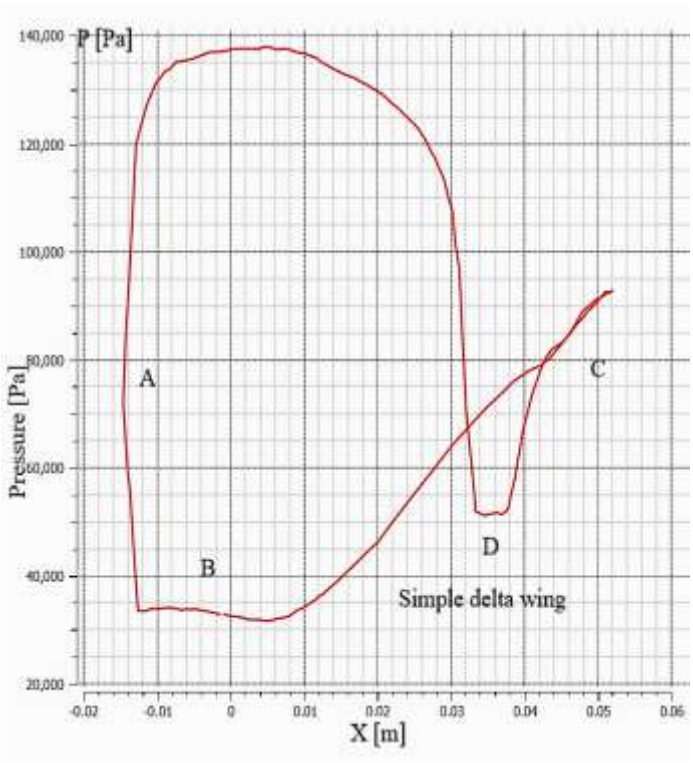

(a)

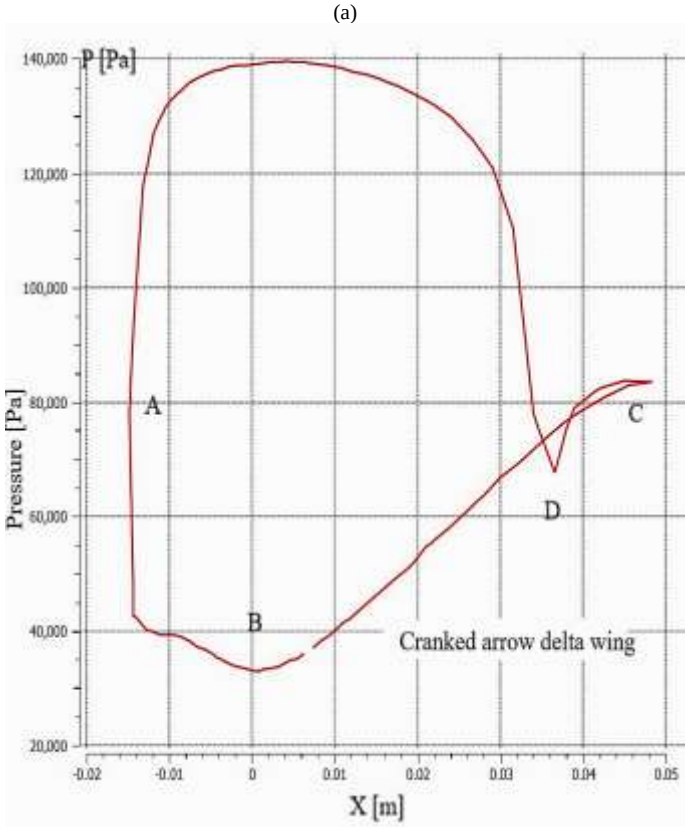

(b)

Figure (19) Pressure distribution at MAC line, $\alpha = 35°$ and $M_\infty = 0.8$

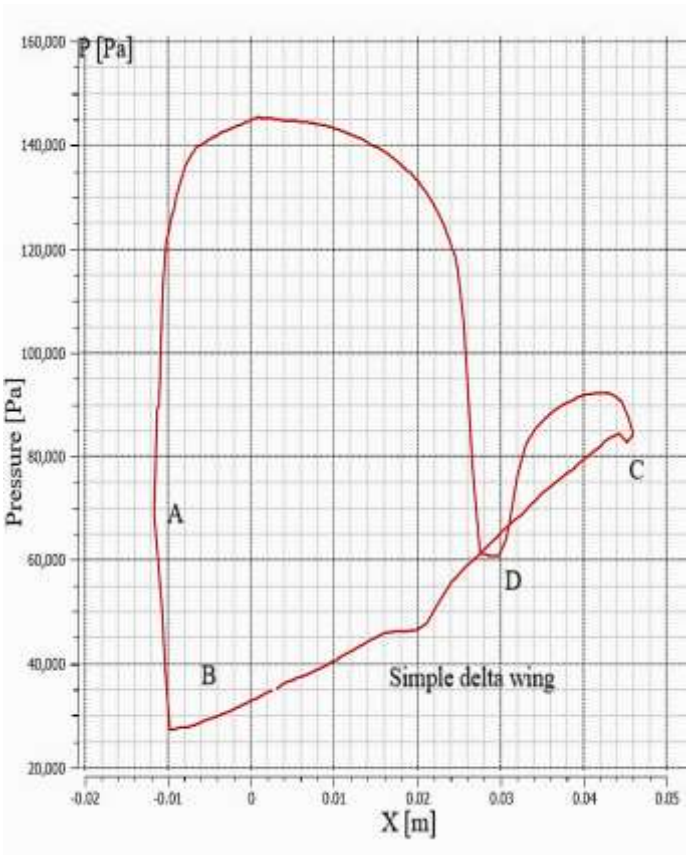

(a)

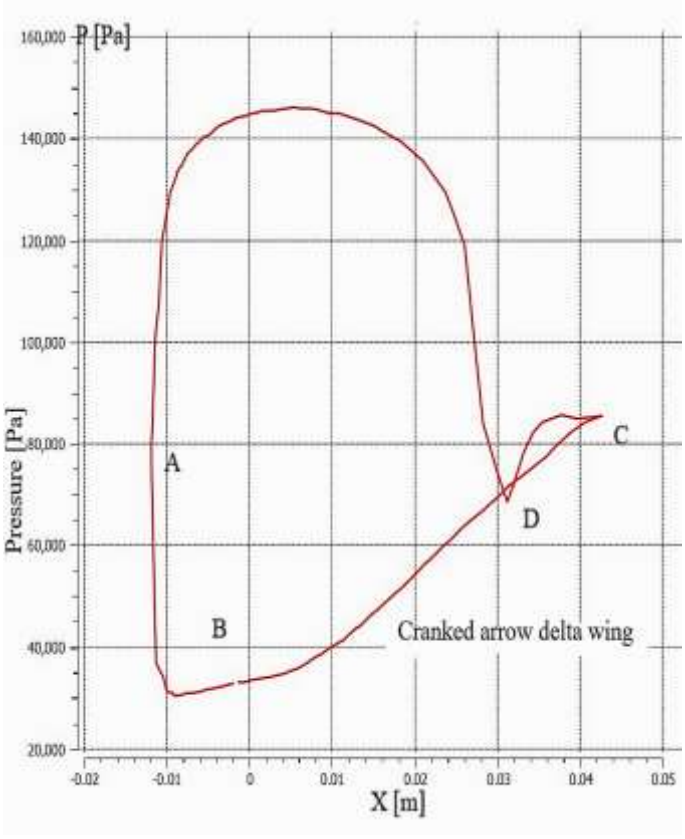

(b)

Figure (20) Pressure distribution at MAC line, $\alpha = 45°$, $M_\infty = 0.8$

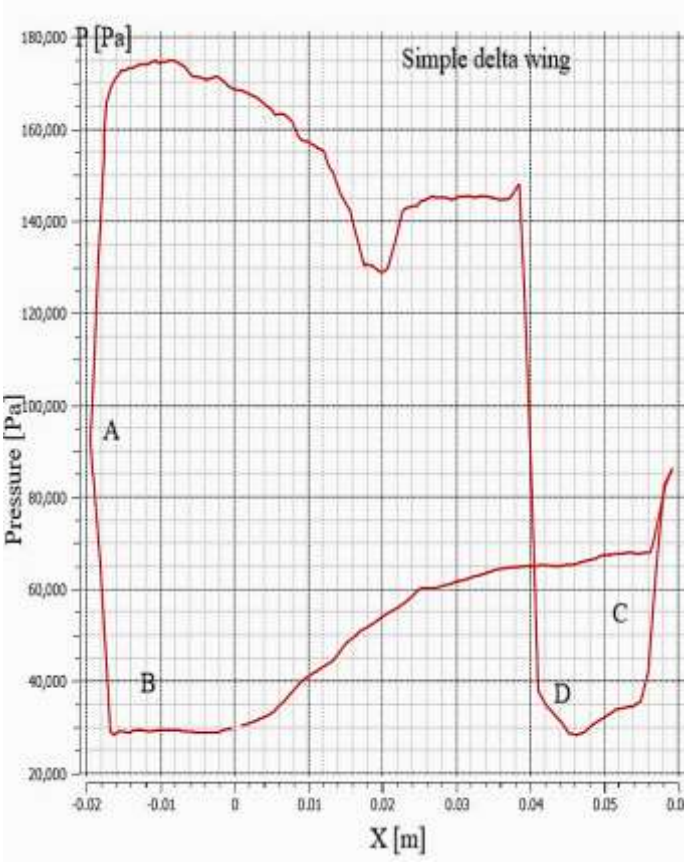

(a)

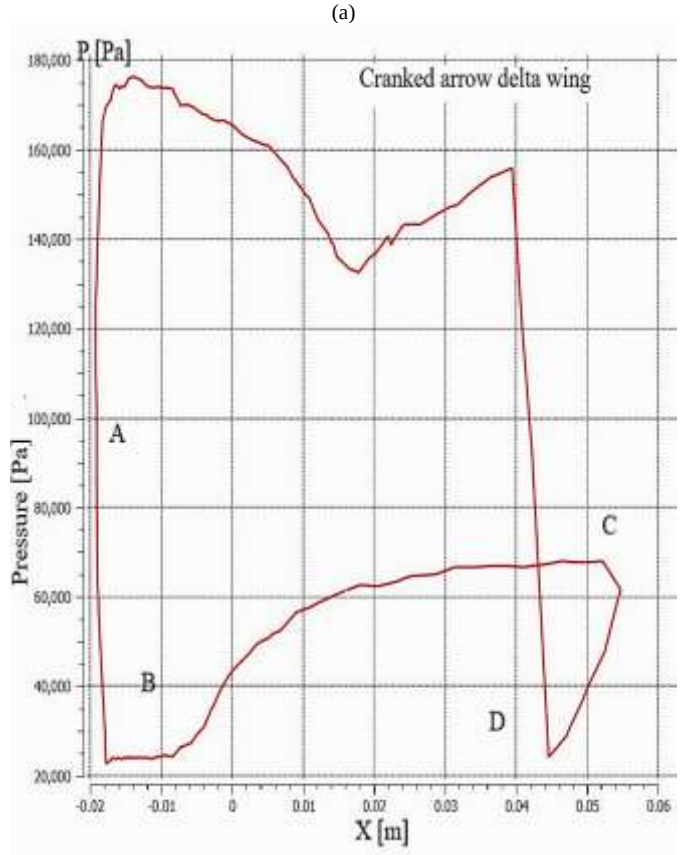

(b)

Figure (21) Pressure distribution at MAC line, $\alpha = 15°$, $M_\infty = 1.4$

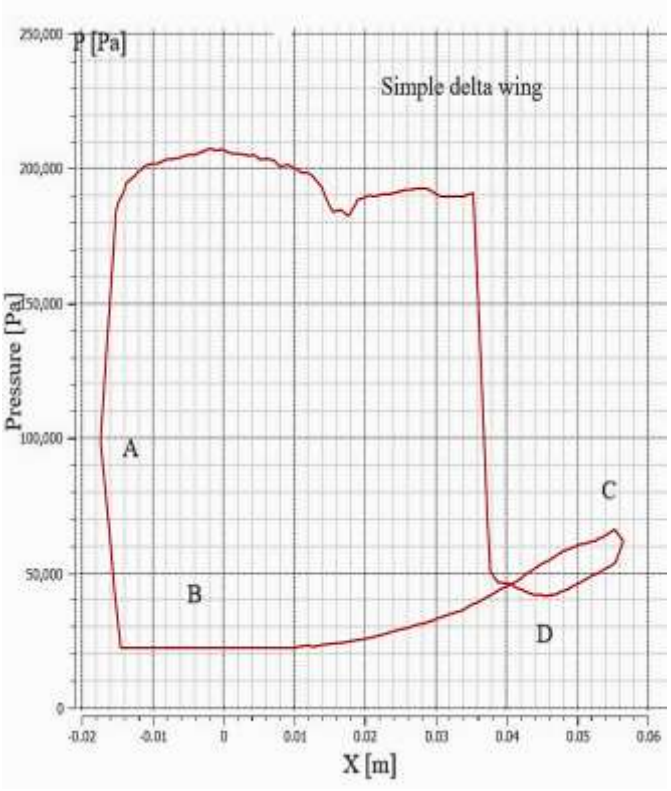

(a)

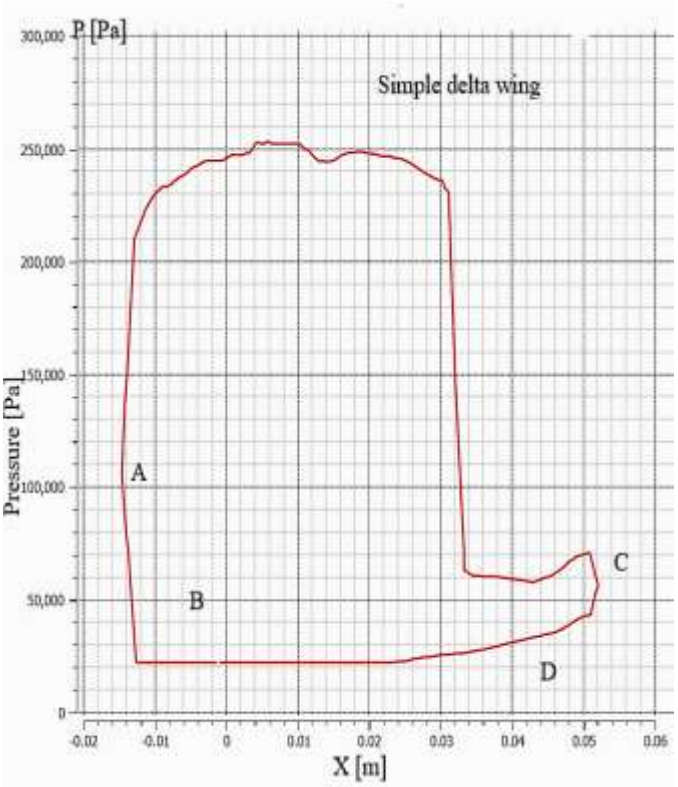

(a)

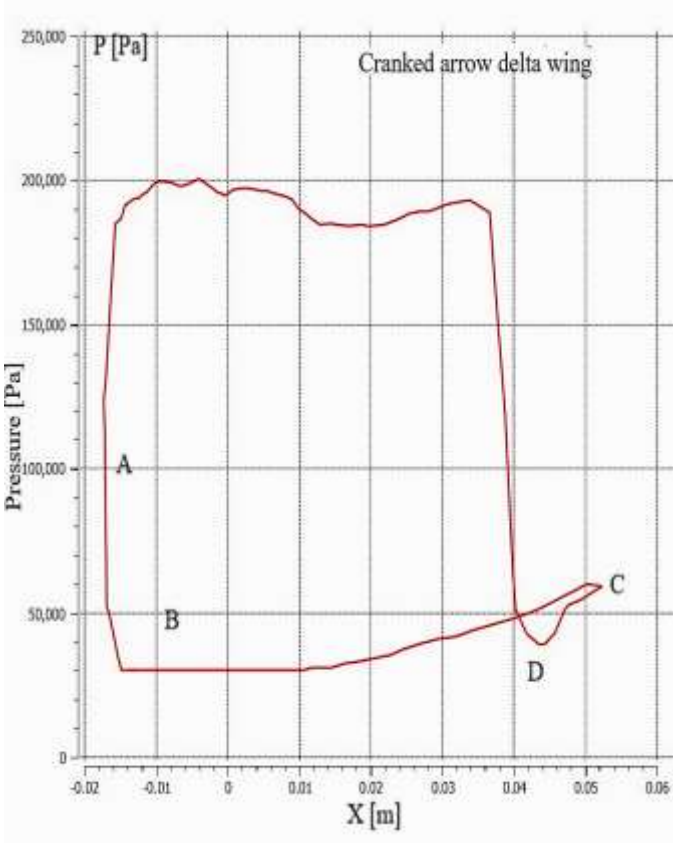

(b)

Figure (22) Pressure distribution at MAC line, $\alpha = 25°$, $M_\infty = 1.4$

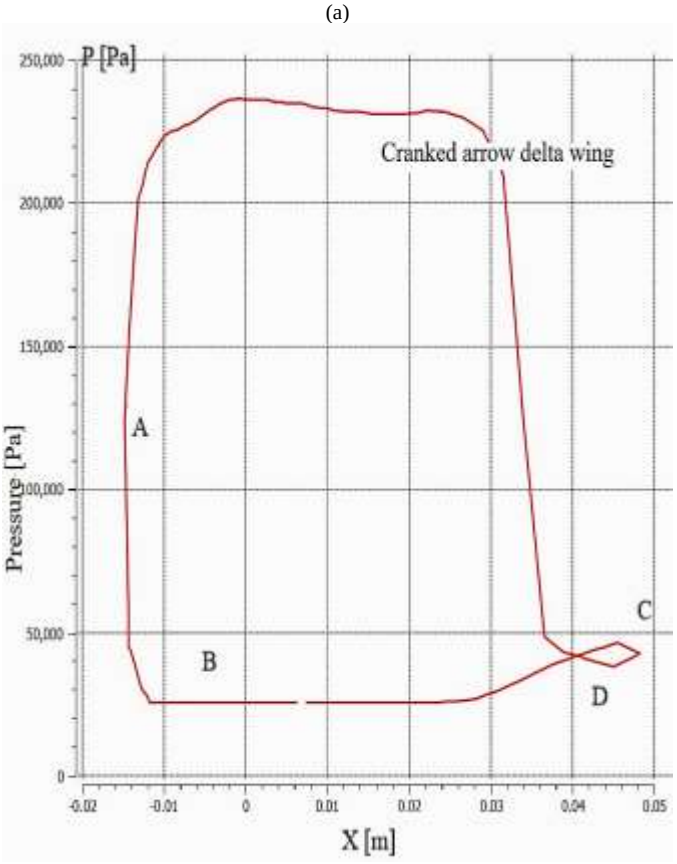

(b)

Figure (23) Pressure distribution at MAC line, $\alpha = 35°$, $M_\infty = 1.4$

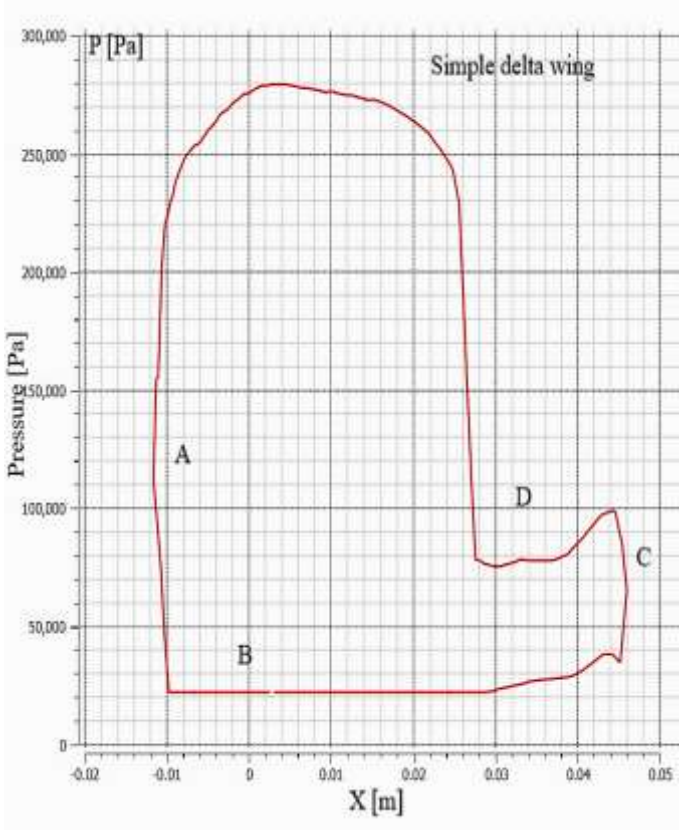

(a)

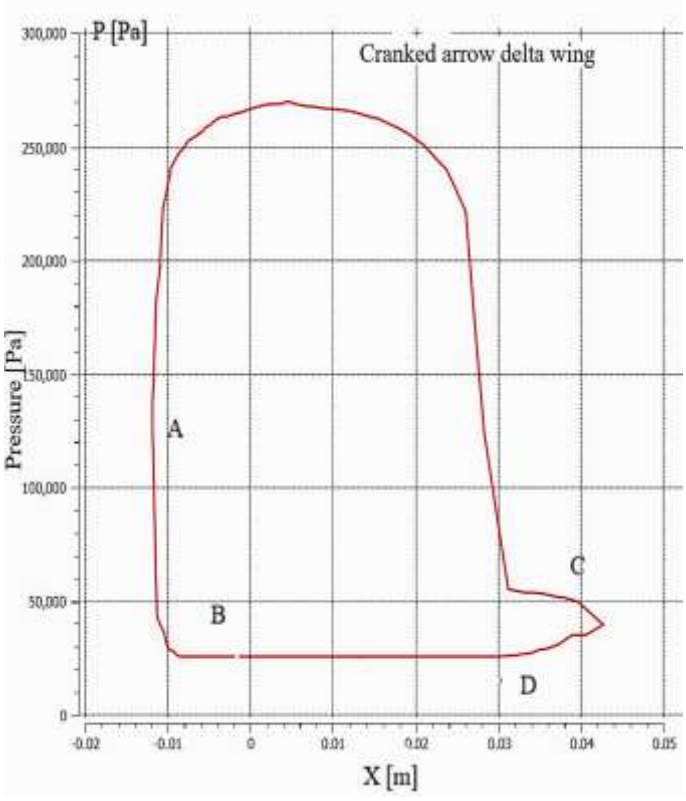

(b)

Figure (24) Pressure distribution at MAC line, $\alpha = 45°$, $M_\infty = 1.4$

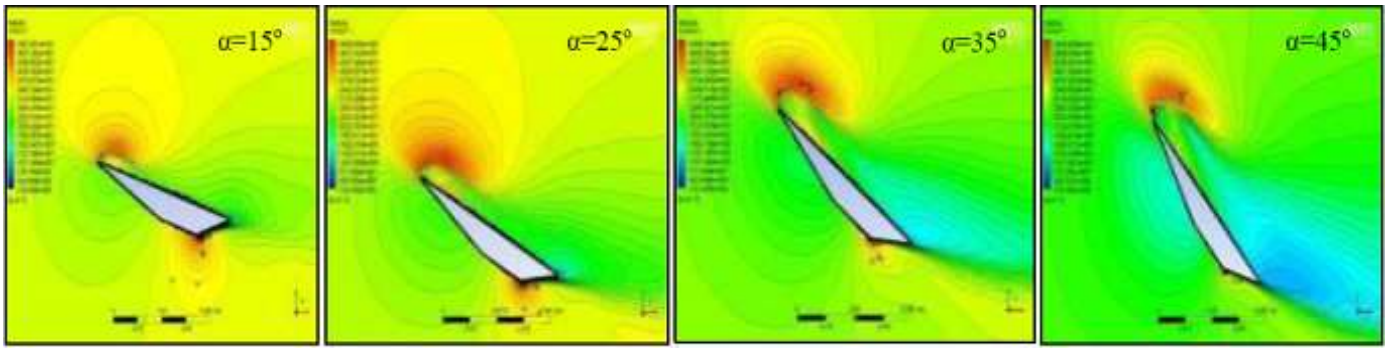

(a) Simple Delta Wing

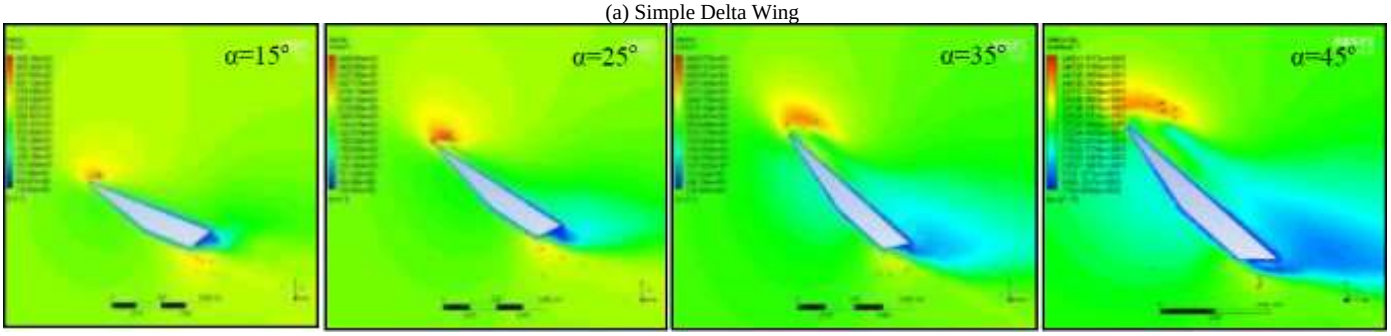

(b) Cranked Arrow delta

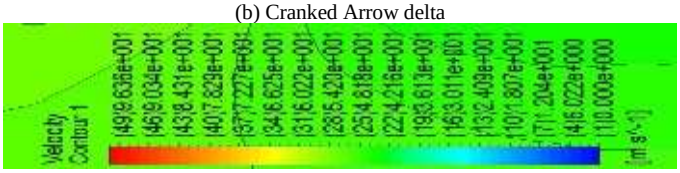

Figure (25) Velocity contours at MAC line for simple delta wing and cranked arrow delta wing, Mach number $M_\infty = 0.15$, α = 15°, 25°, 35°, 45°

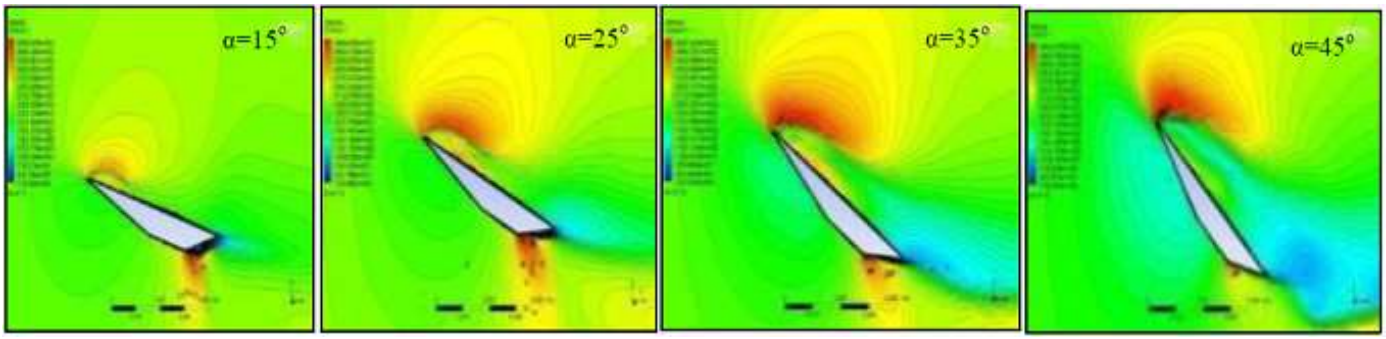

(a) Simple Delta Wing

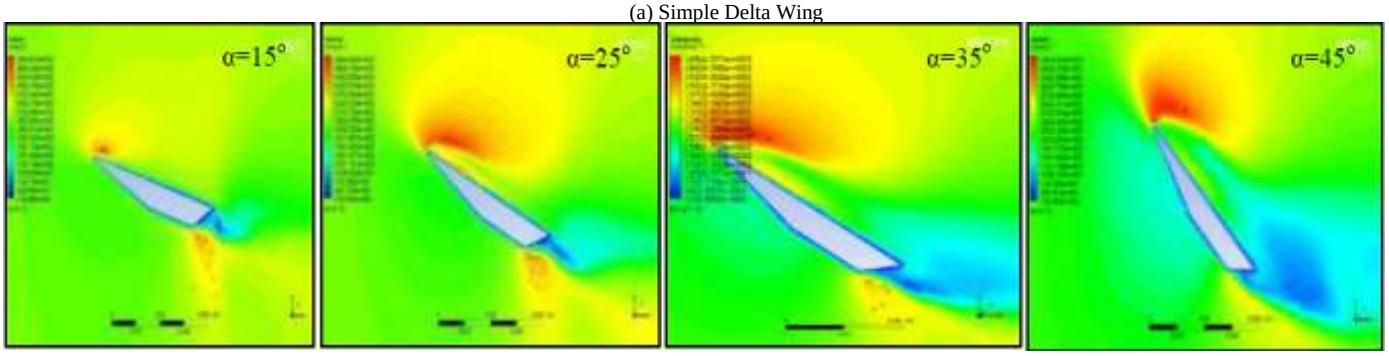

(b) Cranked Arrow Delta wing

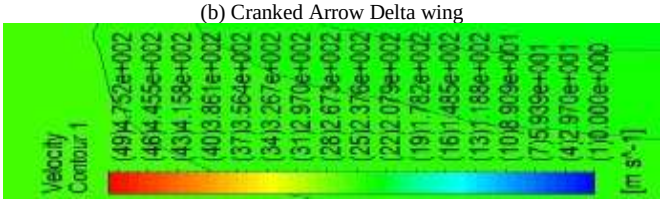

Figure (26) Velocity contours at MAC line for simple delta wing and cranked arrow delta wing, Mach number $M_\infty = 0.8$, α = 15°, 25°, 35°, 45°

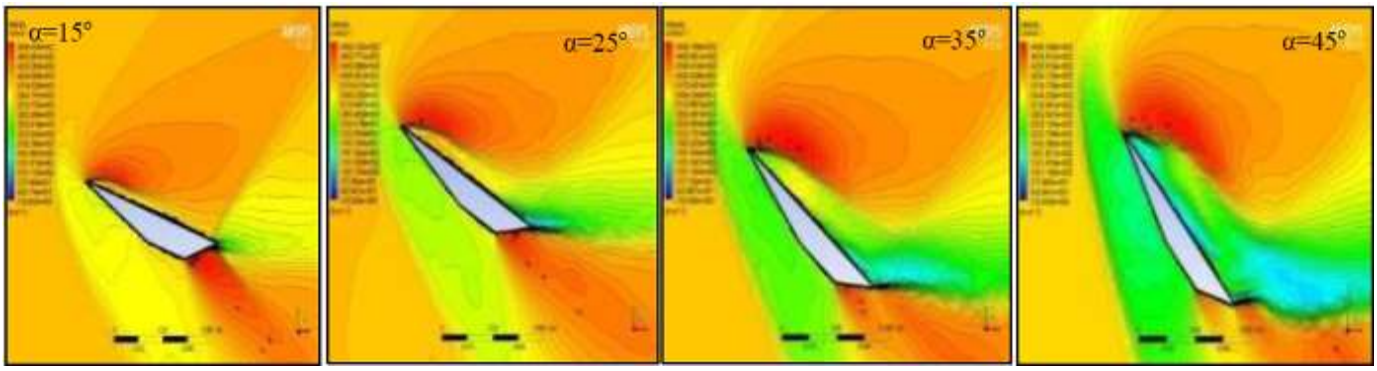

(a) Simple Delta Wing

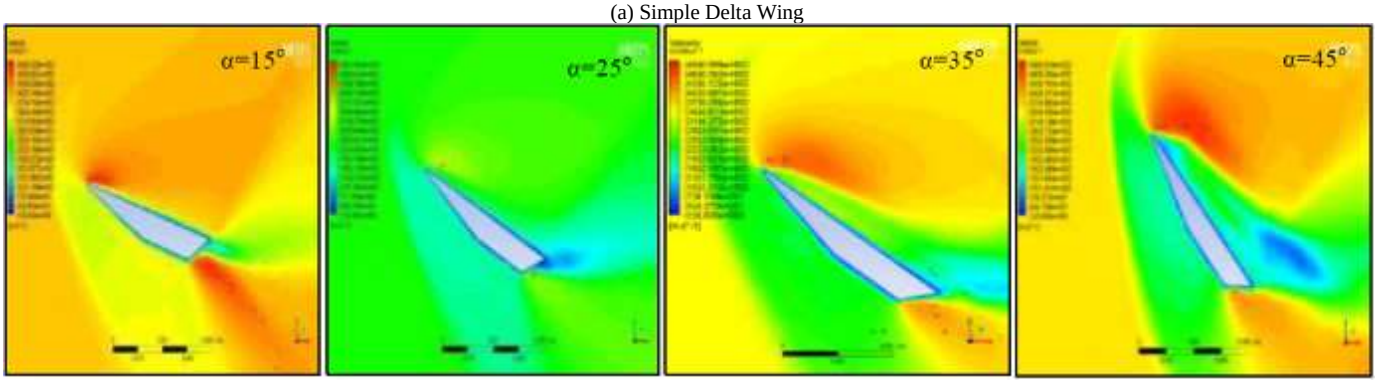

(b) Cranked Arrow Delta Wing

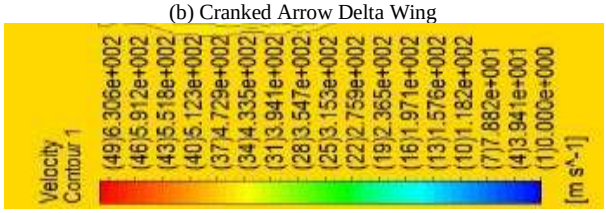

Figure (27) Velocity contours at MAC line for simple delta wing and cranked arrow delta wing, $M_\infty = 1.4$, $\alpha = 15°, 25°, 35°, 45°$

V. CONCLUSION

Through the study of the comparison between the two types of delta wing (simple delta wing and cranked arrow delta wing) in a wide range of subsonic and supersonic speeds (M = 0.15 to 1.4) and different angles of attack (α = 5º to 65º), using ANSYS 15 program and CFD method. The performance of the cranked arrow is better due to the followings:

- With fixing both span and chord in both wings, the area of the cranked arrow is less than the area of simple delta wing by about 7%.
- The lift coefficient is higher for the cranked arrow than that for simple delta wing in both subsonic and supersonic cases.
- Drag forces are lower for the cranked arrow delta wing.
- Increasing Mach number leads to a better pressure distribution over the wing surface of the cranked arrow.
- In the cranked arrow delta wing, the vortex breakdown is delayed than the vortex breakdown that occurs in the simple delta wing.

Nomenclature

AR	Wing aspect ratio
b	Span
c	Chord
C_D	Drag coefficient
C_L	Lift coefficient
C_P	Pressure coefficient
D	Drag
K_P, K_V	Coefficient ($\approx 2\pi \tan \Lambda$)
L	Lift
M	Mach number
P	Pressure
q	Local flow at a slightly different speed
S	Wing surface area
t	Wing thickness
U	Uniform flow velocity in *x* direction
V	Flight velocity vector
u, *v*, *w*	Fluid velocity component in *x*, *y*, *z* direction
x, *y*, *z*	Cartesian coordinates
y/b	Dimensionless distance

Subscript

N	Normal, Perpendicular
∞	Free Stream

Abbreviations

CFD	Computational Fluid Dynamics
LERX	Leading Edge Root Extension
MAC	Main Aerodynamic Chord
PIV	Particle Image Velocimetry

Greek Symbols

α	Angle of attack
θ	Bevel angle
Λ	Swap angle
μ	Dynamic viscosity
π	Constant(3.1416)
ρ	density

REFERENCES

[1] E.L. Houghton, and P.W. Carpenter, (2003). "Aerodynamics for Engineering Students". Fifth edition. Elsevier.

[2] A. Stanbrook, and L.C. Squire, (1964). "Possible types of flow at swept leading edges," *Aeronautical Quarterly*, Vol. 15, No. 2, pp. 72-82.

[3] P.B. Earnshaw, (1962). "An experimental investigation of the structure of a leading-edge vortex". Aeronautical Research Council Reports and Memoranda, No 3281.

[4] D. Hummel, and P.S. Srinivasan, (1967). "Vortex breakdown effects on the low-speed aerodynamics characteristics of slender delta wings in symmetrical flow," *Journal of the Royal Aeronautical Society*, Vol. 71, No. 676, pp. 319-322.

[5] W.H. Wentz, and D.L. Kohlman, (1971). "Vortex breakdown on slender sharp-edged wings," *Journal of Aircraft*, Vol. 8, No. 3, pp. 156-161.

[6] P.M. Sforza, and M.J. Smorto, (1981). "Streamwise development of the flow over a delta wing," *AIAA Journal*, Vol. 19, No. 7, pp. 833-834.

[7] M. Gad-El-Hak, and R.F. Blackwelder, (1985). "The discrete vortices from a delta wing", *AIAA Journal*, Vol. 23, No. 6, pp. 961-962.

[8] P. Konstadinopoulos, D.T. Mook, and A.H. Nayfeh, (1985). "Subsonic wing rock of slender delta wings", *Journal of Aircraft*, Vol. 22, No. 3, pp. 223-228.

[9] M. Gad-el-Hak, and C.-M. Ho, (1985). "The pitching delta wing," *AIAA Journal*, Vol. 23, No. 11, pp. 1660-1665.

[10] R.D.A. Mehta, and E.R.B. Cantwell, (1988). "Mean flow and turbulence measurements in a half-delta wing," *Vortex Fluid Dynamics Research*, Vol. 4, Issue 2, pp. 123-137.

[11] A. Cenedese, M.L. De Prizio, and G.P. Romano, (1991). "Particle image velocimetry measurements in the wake of a delta wing," American Society of Mechanical Engineers, Fluids Engineering Division (Publication) FED, Vol. 128, pp. 15-21. University of Rome 'La Sapienza', Rome, Italy.

[12] G. Yang, X. Lu, and L. Zhuang, (1999). "Vortex control by the spanwise suction flow on the upper surface of delta wing," *Acta Mechanica Sinica*, Vol. 15, Issue 2, pp. 116-125.

[13] K. Rinoie, (2000). "Experiments on a 60-degree delta wing with rounded leading-edge vortex flaps", *Journal of Aircraft*, Vol. 37, No. 1, pp. 37-44.

[14] M. Jones, and Y. Nakamura, (2006). "Azimuthal vorticity dynamics and vortex breakdown above a delta wing". Collection of Technical Papers - 44th AIAA Aerospace Sciences Meeting, Vol. 21, pp. 15928-15940.

[15] A. Furman, and C. Breitsamter, (2006). "Investigation of flow phenomena on generic delta wing". ICAS-Proceedings - 25th Congress of the International Council of the Aeronautical Sciences, Vol. 2, pp. 978-993.

[16] H. Rahman, S. Khushnood, A. Raza, and K. Ahmad, (2013). "Experimental and computational investigation of delta wing aerodynamics". Proceedings of 2013 10th International Bhurban Conference on Applied Sciences and Technology, Art. No. 6512155, pp. 203-208.

[17] W. Ruffles, and S.M. Dakka, (2016). "Aerodynamic flow characteristics of utilizing delta wing configurations in supersonic and subsonic flight regimes," *Journal of Communication and Computer*, Vol. 13, No. 6, pp. 299-318.

[18] I. Sutrisno, T.A. Rochmat, B.W. Setyawan, S. Iswahyudi, C. Wiratama, and W. Kartika, (2018). "The flow visualization CFD studies of the fuselage and rolled-up vortex effects of the chengdu J-10-like fighter canard," *Modern Applied Science*; Vol. 12, No. 2; pp. 148-163.

[19] D. Baldacchino, M. Manolesos, C. Ferreira, Á.G. Salcedo, M. Aparicio, T. Chaviaropoulos, K. Diakakis, L. Florentie, N.R. García, G. Papadakis, N.N. Sørensen, N. Timmer, N. Troldborg, S. Voutsinas, and A. van Zuijlen, (2016). "Experimental benchmark and code validation for airfoils equipped with passive vortex generators," *Journal of Physics: Conference series*, Vol. 753, No. 2, p. 022002.

[20] M.S. Genc, G. Özden, M. Özden, M.S. Kırıs, and R. Yıldız, (2017). "Interaction of tip vortex and laminar separation bubble over wings with different aspect ratios under low Reynolds numbers," *Proceedings of the institution of Mechanical Engineers, Part C: Journal of Mechanical Engineering Science*, Vol. 232, No. 22, pp. 4019-4037.

[21] A. Altman, (2019). "Learning Intro to Flight Course Content through an Individual Aircraft Conceptual Sizing Experience," Conference: AIAA Scitech 2019 Forum, AIAA 2019-0068.

[22] A.P.S. Rathore, (2018). "Aerodynamic characteristics of diamond shaped airfoil at supersonic speed," *International Journal of Aerospace and Mechanical Engineering*, Vol. 5, No. 2, pp. 19-22.

[23] E.C. Pohlhamus, (1968). "A concept of the vortex lift on sharp-edge delta wing based on a leading edge–suction analogy", NASA TN:D-3467.

[24] A. Oyama, G. Imai, A. Ogawa, and K. Fujii, (2008). "Aerodynamic characteristics of a delta wing at high angles of attack," 15th AIAA International Space Planes and Hypersonic Systems and Technologies Conference, 28 April - 1 May 2008, Dayton, Ohio.

[25] D.S. Miller, and R.M. Wood, (1984). "Lee side flows over delta wings at supersonic speeds," *Journal of Aircraft*, Vol. 21, No. 9, pp. 680-686.

[26] A.K. Sawheny, (1989). "A course in Mechanical Measurements and Instrumentation," Third edition. Delhi : Dhanpat Rai and Sons.